



# NIH Public Access

## Author Manuscript

Biochemistry. Author manuscript; available in PMC 2012 November 29.

Published in final edited form as:

*Biochemistry*. 2011 November 29; 50(47): 10262–10274. doi:10.1021/bi201436n.

## Oxy-Intermediates of Homoprotocatechuate 2,3-Dioxygenase: Facile Electron Transfer Between Substrates

Michael M. Mbughuni<sup>†,¤</sup>, Mrinmoy Chakrabarti<sup>‡</sup>, Joshua A. Hayden<sup>‡</sup>, Katlyn K. Meier<sup>‡</sup>, Joseph J. Dalluge<sup>§</sup>, Michael P. Hendrich<sup>\*,‡</sup>, Eckard Münck<sup>\*,‡</sup>, and John D. Lipscomb<sup>\*,†,¤</sup>

<sup>†</sup>Department of Biochemistry, Molecular Biology and Biophysics, University of Minnesota, Minneapolis, Minnesota 55455

<sup>§</sup>Department of Chemistry, University of Minnesota, Minneapolis, Minnesota 55455

<sup>\*</sup>Center for Metals in Biocatalysis, University of Minnesota, Minneapolis, Minnesota 55455

<sup>‡</sup>Department of Chemistry, Carnegie Mellon University, Pittsburgh, Pennsylvania 15213.

### Abstract

Substrates homoprotocatechuate (HPCA) and O<sub>2</sub> bind to the Fe<sup>II</sup> of Homoprotocatechuate 2,3-dioxygenase (FeHPCD) in adjacent coordination sites. Transfer of an electron(s) from HPCA to O<sub>2</sub> via the iron is proposed to activate the substrates for reaction with each other to initiate aromatic ring cleavage. Here, rapid-freeze-quench methods are used to trap and spectroscopically characterize intermediates in the reactions of the HPCA complexes of FeHPCD and the variant His200Asn (FeHPCD-HPCA and H200N-HPCA) with O<sub>2</sub>. A blue intermediate forms within 20 ms after mixing O<sub>2</sub> with H200N-HPCA (H200N<sub>Int1</sub><sup>HPCA</sup>). Parallel mode EPR and Mössbauer spectroscopies show that this intermediate contains high-spin Fe<sup>III</sup> (*S*=5/2) antiferromagnetically coupled to a radical (*S*<sub>R</sub>=1/2) to yield an *S*=2 state. Together, optical and Mössbauer spectra of the intermediate support assignment of the radical as an HPCA semiquinone, implying that oxygen is bound as a (hydro)peroxo ligand. H200N<sub>Int1</sub><sup>HPCA</sup> decays over the next 2 s, possibly through an Fe<sup>II</sup> intermediate (H200N<sub>Int2</sub><sup>HPCA</sup>), to yield product and the resting Fe<sup>II</sup> enzyme. Reaction of FeHPCD-HPCA with O<sub>2</sub> results in rapid formation of a colorless Fe<sup>II</sup> intermediate (FeHPCD<sub>Int1</sub><sup>HPCA</sup>). This species decays within 1 s to yield the product and the resting enzyme. The absence of a chromophore from a semiquinone or evidence for a spin-coupled species in FeHPCD<sub>Int1</sub><sup>HPCA</sup> suggests it is an intermediate occurring after O<sub>2</sub> activation and attack. The similar Mössbauer parameters for FeHPCD<sub>Int1</sub><sup>HPCA</sup> and H200N<sub>Int2</sub><sup>HPCA</sup> suggest these are similar intermediates. The results show that electron transfer from the substrate to the O<sub>2</sub> via the iron does occur leading to aromatic ring cleavage.

---

Extradiol dioxygenases are a class of nonheme Fe<sup>II</sup>- (or occasionally Mn<sup>II</sup>-) containing enzymes that catalyze the cleavage of catecholic substrates adjacent to the vicinal OH functions with incorporation of both atoms of oxygen from O<sub>2</sub> (Scheme 1).<sup>1–5</sup> This reaction allows a host of aerobic microorganisms to channel carbon from naturally occurring and man-made aromatic compounds into the TCA cycle, facilitating biodegradation.<sup>1,4,6,7</sup> As

\*Corresponding Authors To whom correspondence should be addressed: Dr. John D. Lipscomb, Dept. of Biochemistry, Molecular Biology, and Biophysics, 6-155 Jackson Hall, University of Minnesota, 321 Church St. SE, Minneapolis, MN 55455. Phone: 612-625-6454; Fax: 612-624-5121; Lipsc001@umn.edu.. \*Eckard Münck, Department of Chemistry, Carnegie Mellon University, 4400 Fifth Ave., Pittsburgh, Pennsylvania 15213; EMunck@cmu.edu. Phone: 412-268-5058. Michael P. Hendrich, Department of Chemistry, Carnegie Mellon University, 4400 Fifth Ave., Pittsburgh, Pennsylvania 15213; Hendrich@andrew.cmu.edu Phone: (412) 268-1058. Fax: (412) 268-1061..

Supporting Information. Methods for mass spec analysis of <sup>17</sup>O-C3-HPCA; Tables S1-S2; Figures S1-S2. This material is available free of charge via the Internet at <http://pubs.acs.org>.

such, the catechol ring-cleaving dioxygenases have roles in human health and maintenance of the global carbon cycle.

Extradiol dioxygenases were the first members of the large class of so called 2-His-1-carboxylate facial triad enzymes to be recognized.<sup>8</sup> This enzyme class utilizes two His and one Asp/Glu residues to bind the divalent metal through one face of the coordination surface, leaving the other face free to bind solvents or reaction substrates.<sup>9,10</sup> Often a substrate or cofactor will bind to, or very near, the metal causing release of the solvents and opening a coordination site for O<sub>2</sub> (see examples<sup>11</sup>). It has been shown that, in the case of the extradiol dioxygenases, the catecholic substrates and O<sub>2</sub> bind to the metal in adjacent coordination sites (Scheme 1 A-D).<sup>12</sup> We and others have proposed that electron transfer from the substrate to the oxygen via the metal gives radical character to both the substrate and the oxygen (Scheme 1 B-D).<sup>1,10,12-14</sup> Recombination of the radicals to form a metal-bound alkylperoxo intermediate would initiate aromatic ring cleavage (Scheme 1 E-G).

An oxygen activation mechanism of this type does not require a formal change in oxidation state of the metal between the initial enzyme-aromatic substrate complex and postulated diradical reactive state (Scheme 1 D). Accordingly, it has recently been shown that the recombinant extradiol dioxygenase Homoprotocatechuate 2,3-dioxygenase originally isolated from *Brevibacterium fuscum* (FeHPCD, Scheme 1) functions with the same  $k_{cat}$ , and  $k_{cat}/K_mO_2$  values within error when the Fe<sup>II</sup> is replaced by Mn<sup>II</sup> (MnHPCD).<sup>15</sup> It exhibits even higher  $k_{cat}$  and  $K_mO_2$  values when Co<sup>II</sup> is substituted.<sup>16</sup> The fact that the enzyme is fully functional using metals with a redox potential range spanning 1.15 V suggests either no change in metal oxidation state or no net change between the enzyme form that can bind O<sub>2</sub> and that which can irreversibly attack substrate. An indication that the metal transiently changes redox state prior to formation of the reactive species has come from a kinetic study of the reaction of MnHPCD with the natural substrate (HPCA) and O<sub>2</sub>.<sup>17</sup> A species best described as Mn<sup>III</sup>-O<sub>2</sub><sup>•-</sup> is formed in low yield and then decays to a Mn<sup>II</sup> species within 30 ms of the start of the reaction. This second intermediate may be the alkylperoxo intermediate of the reaction cycle, which then decays to yield ring-cleaved product.

Investigation of the native FeHPCD mechanism has been facilitated by discovery of methods to slow the rates of steps in the reaction cycle. One method has been to conduct the reaction in a single crystal using the slowly cleaved substrate, 4-nitrocatechol (4NC). It was found that the postulated 4NC-semiquinone (SQ<sup>•</sup>)-Fe<sup>II</sup>-O<sub>2</sub><sup>•-</sup> (Scheme 1D) and Fe<sup>II</sup>-alkylperoxo-(Scheme 1E) intermediates, as well as the ring-cleaved product intermediate (Scheme 1G) were stabilized in different active sites of the asymmetric unit of the crystal.<sup>12</sup> This allowed them to be structurally characterized. Another approach to slow the reaction was to use active site variants of the postulated active site acid/base catalyst His200.<sup>18,19</sup> It was found when His200 was replaced by Asn (H200N), and 4NC was used as the substrate, O<sub>2</sub> bound to form a long-lived, antiferromagnetically coupled Fe<sup>III</sup>-O<sub>2</sub><sup>•-</sup> species (H200N<sub>Int1</sub><sup>4NC</sup>). This species decayed during the following 100 s to another intermediate (H200N<sub>Int2</sub><sup>4NC</sup>) postulated to be a 4NC SQ<sup>•</sup>-Fe<sup>III</sup>-peroxy species. Rather than undergo ring cleavage, this intermediate decayed to release 4NC quinone and H<sub>2</sub>O<sub>2</sub> and restore the Fe<sup>II</sup> center of the enzyme. This study showed that a change in the iron redox state can occur as O<sub>2</sub> binds, but the downstream chemistry deviates from normal catalysis, suggesting that the H200N mutation and/or the use of a substrate with an electron withdrawing substituent can uncouple O<sub>2</sub> activation from ring cleaving chemistry.

Transient kinetic studies of extradiol dioxygenase reactions that yield the correct ring-cleaved products have been carried out using HPCA as the substrate for FeHPCD and H200N.<sup>18,20</sup> These studies revealed at least four intermediates following addition of O<sub>2</sub> with a pre-formed enzyme-substrate complex. In the case of H200N, the O<sub>2</sub> binding step itself

could be monitored because a visible absorption band associated with the complex was observed near 610 nm.

In the current study, we use rapid-freeze-quench (RFQ) methods to trap and spectroscopically characterize the intermediates from the reaction of FeHPCD- and H200N-HPCA complexes with O<sub>2</sub>. The earliest trapped intermediates differ markedly from that identified in the H200N-4NC reaction with O<sub>2</sub>.<sup>19</sup> Together, they support a mechanism in which facile electron transfer between bound HPCA and O<sub>2</sub> via the Fe<sup>II</sup> forms the basis for O<sub>2</sub> activation and insertion chemistry.

## EXPERIMENTAL PROCEDURES

### Reagents and Enzymes

All chemicals were purchased from Sigma-Aldrich and were used without purification except for HPCA which was recrystallized from water at 4 °C to remove minor contaminants. Anaerobic conditions were achieved by repeated cycling of solutions between argon gas and vacuum. Trace contaminating O<sub>2</sub> was removed from the Ar gas by passage through an Agilent GC-1 POP O<sub>2</sub> scrubbing cartridge, then through an Agilent GC-4 POP O<sub>2</sub> indicating cartridge. Formate dehydrogenase (FDH) was prepared as previously described.<sup>21</sup> The C<sub>1</sub> and C<sub>2</sub> *p*-hydroxyphenylacetate hydroxylase system from *Acinetobacter baumannii* was the generous gift of David P. Ballou. Recombinant *Brevibacterium fuscum* FeHPCD and the H200N variant were expressed and purified as previously described.<sup>18,22</sup> <sup>57</sup>Fe-enriched enzyme was prepared for RFQ/ Mössbauer experiments as previously described.<sup>19</sup> Mushroom Tyrosinase was purchased from Sigma.

### Stopped-flow and Spectroscopy

All stopped-flow experiments were performed using an Applied Photophysics model SX. 18MV stopped flow device at 4 °C. The reaction procedures were as previously described.<sup>20</sup> The kinetic data were analyzed to extract reciprocal relaxation times using the Applied Photophysics Pro-Data Viewer version 4.0.17. EPR spectra were collected using a Bruker Elexsys E-500 or Bruker ESP 300 spectrometer each equipped with a Bruker dual mode cavity and an Oxford ESR 910 liquid helium cryostat. Mössbauer spectroscopy was performed as previously described.<sup>19,23</sup> Spectra were analyzed using the software WMOSS (SEE Co, Edina, MN, USA).

### RFQ Methods

Anaerobic substrate complexes were prepared in a Coy glovebox as previously described.<sup>19</sup> RFQ syringes were loaded inside the anaerobic glovebox before transferring to the Update RFQ Instrument (Model 1019 RFQ) where they were equilibrated at 4 °C for 30 min using an ice bath. After rapid mixing and passage through a calibrated delay line, samples were collected by rapid freezing on counter-rotating aluminum wheels at Liq N<sub>2</sub> temperature. A programmed delay was used for time points > 0.4 s. For samples at times > 1.5 s, the mixed sample was collected directly in an EPR tube or Mössbauer cup and frozen by rapid emersion in a dry ice/methanol bath (EPR) or Liq N<sub>2</sub> (Mössbauer) after the appropriate incubation time. We have observed that freezing on the counter-rotating wheels introduces a small splash artifact that becomes more prominent at the highest ram drive speeds. The splashed material falls into the Liq N<sub>2</sub> bath directly and freezes more slowly than the material on the wheel, causing the appearance of the spectrum of the product complex in early samples. The rate of product formation for the reactions investigated here is well known from stopped flow experiments,<sup>20</sup> and no product-complex is expected in the earliest RFQ samples collected.

## Synthesis of HPCA Enriched with $^{17}\text{O}$ at the C3 Hydroxyl Functional Group

$3\text{-}^{17}\text{OH-HPCA}$  was prepared from p-hydroxyphenylacetate (HPA). The  $\text{C}_1$  and  $\text{C}_2$  hydroxylase from *Acinetobacter baumannii*<sup>24</sup> was used to catalyze conversion of HPA to  $3\text{-}^{(17)\text{OH}},4\text{-}^{(16)\text{OH}}$ -dihydroxyphenylacetic using 70% enriched  $^{17}\text{O}_2$  (Cambridge Isotopes). A 2 mL reaction mixture was prepared in a 5 mL pear shaped flask fitted with a 3-way valve in the anaerobic glovebox. Concentrations of the reactants were 10  $\mu\text{M}$   $\text{C}_1$ , 20  $\mu\text{M}$   $\text{C}_2$ , 20  $\mu\text{M}$  FDH, 100  $\mu\text{M}$  NADH, 15 mM formate, and 10 mM HPA. The flask mouth was capped with a SUBA seal septa crimped with copper wire and the valve closed prior to removal from the glovebox. The 3-way valve was connected to a vacuum/argon line and to a tank of 70% enriched  $^{17}\text{O}_2$  and the lines were evacuated and exchanged with argon several times. The system was opened to vacuum and the head space of the pear shape flask evacuated for  $\sim 1$  s. The vacuum line was closed and the flask was filled with 1-2 psi of 70% enriched  $^{17}\text{O}_2$  to initiate the reaction. The reaction was allowed to proceed for 2 h at room temperature to reach completion, and then it was quenched with 3%  $\text{H}_2\text{SO}_4$ . The quenched reaction was centrifuged at  $39,000 \times g$  for 40 min to remove insoluble materials. The supernatant from centrifugation was assayed for HPCA using the catalytic activity of FeHPCD which converts HPCA to the  $\alpha$ -hydroxy  $\delta$ -carboxymethyl *cis*-muconic semialdehyde, which has an extinction coefficient at 380 nm of  $38,000 \text{ M}^{-1} \text{ cm}^{-1}$ .<sup>20</sup> The assay revealed nearly stoichiometric conversion of HPA to HPCA. The reaction supernatant containing  $3\text{-}^{17}\text{OH-HPCA}$  was lyophilized and then dissolved in 50 mM MOPS buffer pH 7.5 and stored at -80 °C until used in RFQ experiments. LC/MS/MS analysis of the synthesized HPCA is described in *Supplemental Materials* and shows nearly 68% enrichment of one atom of  $^{17}\text{O}$  per HPCA molecule.

## Preparation of HPCA Quinone

HPCA was oxidized using mushroom tyrosinase (Sigma) in 100 mM MES buffer pH 5.6 and 4 °C. The reaction was initiated and monitored using the stopped-flow spectrometer with diode-array detection. A solution of 2 mM HPCA was mixed with 10 mg/ml mushroom tyrosinase. The quinone product formed during the first 5 min of the reaction and then slowly decayed to an unidentified secondary species.

## RESULTS

### Single-Turnover Studies of the H200N-HPCA + O<sub>2</sub> Reaction Reveal a Transient Intermediate

Our previous stop-flow studies revealed the accumulation of at least four reaction cycle intermediates after the pre-formed H200N-HPCA complex reacts with O<sub>2</sub> in a single-turnover reaction.<sup>18</sup> Improvements in the stopped-flow instrumentation and procedures<sup>19</sup> allow the first of these intermediates to accumulate in higher yield so that it can be studied in detail.

As shown in Figure 1A, for the reaction of a stoichiometric (per active site) H200N-HPCA complex with a slight excess of O<sub>2</sub> at pH 7.5, the previously described 610 nm transient intermediate (H200N<sub>Int1</sub><sup>HPCA</sup>,  $\epsilon_{610 \text{ nm}} \sim 1100 \text{ M}^{-1} \text{ cm}^{-1}$ ) rapidly accumulates and then more slowly decays to give the ring-cleaved product ( $\epsilon_{380 \text{ nm}} \sim 38,000 \text{ M}^{-1} \text{ cm}^{-1}$ ). The absorption maximum for product is shifted to 325 nm ( $\epsilon_{325 \text{ nm}} \sim 23,600 \text{ M}^{-1} \text{ cm}^{-1}$ ) when the reaction is conducted at pH 5.5, allowing a second maximum in the spectrum of H200N<sub>Int1</sub><sup>HPCA</sup> to be observed near 395 nm ( $\epsilon_{395 \text{ nm}} \sim 3200 \text{ M}^{-1} \text{ cm}^{-1}$ ) (Figure 1B). These same features plus an additional feature at 310 nm are revealed by subtracting the 3 ms spectrum from the 32 ms spectrum for the reaction at pH 7.5 (Figure 1A, inset). When the reaction is conducted at pseudo first-order concentrations of O<sub>2</sub> at pH 7.5 (Figure S1), the time course can be fit well by a two-summed exponential equation with reciprocal relaxation times of  $1/\tau_1 = 230 \pm 20$

$s^{-1}$  and  $1/\tau_2 = 1.6 \pm 0.2 s^{-1}$  showing that the reaction consists of at least two steps. The spectroscopic data reported below shows that the intermediate builds to nearly stoichiometric yield. The observed value of  $1/\tau_1$  is linearly dependent on  $O_2$  concentration with a zero intercept,<sup>18</sup> suggesting that the reaction is irreversible  $O_2$  binding with a  $1/\tau_1 = k_{\text{form}} = k_1$ . The formation of the alkylperoxo intermediate and the ring-cleaving reaction are also likely to be irreversible so that  $1/\tau_2 = k_{\text{decay}} = k_2$  for  $H200N_{\text{Int1}}^{\text{HPCA}}$ . At pH 5.5, the reaction is slightly slower due to a decrease in  $k_2$  ( $k_1 = 240 \pm 20 s^{-1}$  and  $k_2 = 1.1 \pm 0.1 s^{-1}$ ). The two reciprocal relaxation times derived from the fits of the time course at this pH are found to be independent of wavelength when monitored at 310, 395, or 610 nm, suggesting that all features result from  $H200N_{\text{Int1}}^{\text{HPCA}}$ . The spectra of the intermediate change very little in the range between pH 5.5 and 9 (Figure 1B, inset). The reaction could not be monitored at pH values significantly above pH 9 due to structural alterations of the enzyme.

### RFQ EPR and Mössbauer Studies Show that $H200N_{\text{Int1}}^{\text{HPCA}}$ has an $S_1=5/2$ Fe<sup>III</sup> Site Coupled to an $S_R=1/2$ Radical

The anaerobic  $H200N$ -HPCA complexes (see below) contain a high-spin Fe<sup>II</sup> that is EPR-silent in both perpendicular (not shown) and parallel modes (Figure 2, top). The parallel mode EPR spectra of RFQ samples frozen at times between 20 ms and 2 s during the time course of the reaction of this complex with  $O_2$  are shown in Figure 2. At 20 ms, an EPR resonance near  $g = 8.2$  is observed in parallel mode (Figure 2). This feature maximizes at approximately 40 ms and then decays over the course of 2 s.

A superposition of the fit of the 610 nm stopped-flow data from Figure S1 and the  $g = 8.2$  EPR time course is shown in Figure 2, inset. The congruence of these data indicates that the  $g = 8.2$  EPR feature originates from  $H200N_{\text{Int1}}^{\text{HPCA}}$ . Furthermore, the observation of this signal in parallel mode and its absence in perpendicular mode demonstrates that it belongs to a species with integer electronic spin.

The EPR spectrum of  $H200N_{\text{Int1}}^{\text{HPCA}}$  quenched at 40 ms is shown in more detail in Figure 3. The spectrum has contributions from two species, namely,  $H200N_{\text{Int1}}^{\text{HPCA}}$  ( $g = 8.2$ ) and a broader resonance from an Fe<sup>II</sup> species. At 2 K, the  $g = 8.2$  signal intensity is small relative to that of the Fe<sup>II</sup> species. The  $g = 8.2$  feature is significantly larger at 10 K, indicating that it originates from an *excited* spin doublet. The Mössbauer spectra discussed below reveal that the iron of  $H200N_{\text{Int1}}^{\text{HPCA}}$  is high-spin ( $S_1 = 5/2$ ) Fe<sup>III</sup> that resides in a complex with integer spin. The Mössbauer and EPR data are readily reconciled by assuming that  $H200N_{\text{Int1}}^{\text{HPCA}}$  has an  $S_1 = 5/2$  site that is antiferromagnetically (AF,  $J > 0$ ) coupled to an  $S_R = 1/2$  radical. The exchange coupling separates the electric levels into a ground multiplet with  $S = 2$  and an excited state with  $S = 3$ . The  $g = 8.2$  signal originates from the  $M_S = \pm 2$  doublet, at energy  $E \approx 5.4 \text{ cm}^{-1}$ , of the  $S = 2$  multiplet; this doublet is indicated in the level diagram in Figure 3. The electronic levels of the system can be described by the spin Hamiltonian (this is the uncoupled representation):

$$\mathcal{H}_e = JS_1 \bullet \mathbf{S}_R + D_1 \left[ S^2_{1z} - 35/12 + (E/D)_1 (S^2_{1x} - S^2_{1y}) \right] + \beta (\mathbf{S}_1 \bullet \mathbf{g}_1 + \mathbf{S}_R \bullet \mathbf{g}_R) \bullet \mathbf{B}$$

[1]

where the subscripts 1 and R refer to the Fe<sup>III</sup> and the radical, respectively. The exchange coupling ( $J$ ), the zero-field splitting ( $D$ ,  $E$ ) of the ferric ion, and electronic Zeeman terms have their common definitions. Throughout this manuscript we will use isotropic  $g_1 = 2.015$  and  $g_R = 2.00$  (our data are sensitive only to the z-component of the tensors). For describing

the broadening of the  $g = 8.2$  resonance for  $^{17}\text{O}$  enriched samples is advisable (reason given below) to use the  $S = 2$  Hamiltonian (the coupled representation).

$$\mathcal{H}_{S=2} = D \left[ S^2_z - 2 + (E/D) (S^2_x - S^2_y) \right] + \beta B_z g_z S_z + S_z A_z^{O,c} I_z^O \quad [2]$$

The parameters of eq 2 are related to those of eq 1 by:  $D = (4/3)D_1$ ,  $E/D = (E/D)_1$  and  $g_z = (7/6)g_{1z} - (1/6)g_{Rz} \approx 2.00$ . The third term in eq 2 describes the hyperfine interaction of the  $^{17}\text{O}$  nucleus with its electronic environment; where  $A_z^{O,c}$  is expressed in the coupled representation. For the  $^{17}\text{O}_2$  enriched sample, depending on the bonding, there could be one or two  $^{17}\text{O}$  nuclei contributing to the broadening. The spectra are only broadened by the nuclear interaction and do not show resolved splittings, thus the derived value of  $A_z^{O,c}$  assumes one  $^{17}\text{O}$  interaction and is an upper limit (two equivalent  $^{17}\text{O}$  nuclei would reduce  $A_z^{O,c}$  by 25%). The temperature dependence of the  $g = 8.2$   $\text{H}_2\text{O}_2\text{N}_{\text{Int}1}^{\text{HPCA}}$  signal in Figure 3 is plotted as signal times temperature versus temperature. Signal times temperature is proportional to the population of the EPR active doublet, and a fit to the points based on Eq. 1 gives the exchange coupling constant  $J = +25 \text{ cm}^{-1}$ . The rise of the signal at low temperature is due to the increasing population of the  $M_S = \pm 2$  level within the  $S = 2$  multiplet, whereas its decline at higher temperature reflects population of the  $S = 3$  multiplet. The solid line in Figure 3A shows a SpinCount simulation of the  $\text{H}_2\text{O}_2\text{N}_{\text{Int}1}^{\text{HPCA}}$  spectrum using the parameters given in the caption and in Table 1. For  $J/D_1 \approx 25$ , the system is in the strong coupling limit and consists of two well separated  $S = 2$  and  $S = 3$  multiplets. The intensity of the EPR signal (accounting for  $\approx 80\%$  of the iron in the sample) is in approximate agreement with the concentration of the sample; however, due to somewhat variable packing density of the RFQ sample, this concentration has a 10 % uncertainty. Figure 3B shows a simulation of the  $\text{Fe}^{\text{II}}$  species with parameters given in the figure caption. This species accounts for  $\approx 20\%$  of the iron in the sample, and it is not present in the starting  $\text{Fe}^{\text{II}}$  enzyme prior to mixing with substrate and oxygen. Further details of this species are given below.

Figures 4B-E show selected Mössbauer spectra from the time course of the  $\text{H}_2\text{O}_2\text{N}-\text{HPCA}$  reaction with  $\text{O}_2$ ; these spectra were collected at 4.2 K in the absence of an applied magnetic field ( $B = 0$ ). As reported previously, the iron site of  $\text{H}_2\text{O}_2\text{N}$  (Figure 4A) exhibits *one* doublet with quadrupole splitting  $\Delta E_Q = 3.01 \text{ mm/s}$  and isomer shift  $\delta = 1.24 \text{ mm/s}$ ; these parameters are typical of high-spin  $\text{Fe}^{\text{II}}$  with octahedral O/N coordination.<sup>19</sup> The anaerobically prepared, stoichiometric  $\text{H}_2\text{O}_2\text{N}-\text{HPCA}$  sample of Figure 4B exhibits two high-spin ferrous species, namely  $\text{H}_2\text{O}_2\text{N}_{\text{ES}1}^{\text{HPCA}}$  (green, 60% of Fe) with  $\Delta E_Q = 3.45 \text{ mm/s}$ ,  $\delta = 1.16 \text{ mm/s}$  and  $\text{H}_2\text{O}_2\text{N}_{\text{ES}2}^{\text{HPCA}}$  (blue, 40%) with  $\Delta E_Q = 2.32 \text{ mm/s}$ ,  $\delta = 1.20 \text{ mm/s}$  (see also Table 2). Samples prepared with a 2-fold excess of substrate or at pH 6 displayed the same species in the same ratio. (footnote 2) Within 20 ms after mixing the  $\text{H}_2\text{O}_2\text{N}-\text{HPCA}$  complex(es) with stoichiometric amounts of  $\text{O}_2$ , both doublets have disappeared. The 20 ms spectrum is dominated by a new species (representing  $\sim 75\%$  of the Fe) with  $\Delta E_Q = 0.95 \text{ mm/s}$  and  $\delta = 0.48 \text{ mm/s}$ . This species, called  $\text{H}_2\text{O}_2\text{N}_{\text{Int}1}^{\text{HPCA}}$ , has a  $\delta$  value typical of high-spin  $\text{Fe}^{\text{III}}$  ( $S_1 = 5/2$ ). The observation of a quadrupole doublet at 4.2 K in zero field, rather than a spectrum exhibiting paramagnetic hyperfine structure as is usual for isolated  $\text{Fe}^{\text{III}}$ , suggests that  $\text{H}_2\text{O}_2\text{N}_{\text{Int}1}^{\text{HPCA}}$  has an overall zero or integer spin. This is consistent with the formulation of  $\text{H}_2\text{O}_2\text{N}_{\text{Int}1}^{\text{HPCA}}$  that emerged from our EPR studies. Ca 20-25% of the iron in 20 ms the sample belongs to an  $\text{Fe}^{\text{II}}$  species, perhaps multiple species, with  $\Delta E_Q \approx 3.10 \text{ mm/s}$  and  $\delta \approx 1.20 \text{ mm/s}$  (this species may give rise to the broad integer spin EPR

<sup>2</sup>The origin of the two enzyme-substrate species remains unknown. Crystal structures of enzyme-substrate complexes show that the small molecule ligand site of the iron has variable solvent occupancy, offering a possible source of the heterogeneity.

spectrum of Figure 3B). As pointed out in *Experimental Procedures*, at high mixing speeds some of the material bounces off the aluminum wheel of the quencher and cools more slowly, leading to the appearance of later species in earlier time point samples. Our kinetic data indicate that the reaction has not progressed appreciably beyond H200N<sub>Int1</sub><sup>HPCA</sup> at 40 ms under the experimental conditions (Figure S2), suggesting that the ferrous species in the 20 ms sample, which differ(s) from the substrate complexes, arises from this “splashed” material. A spectrum recorded for a sample quenched at 40 ms (not shown) was identical to the one obtained at 20 ms, showing that the amount of material attributed to splash is constant, as expected. At 400 ms, the fraction of iron in H200N<sub>Int1</sub><sup>HPCA</sup> has decreased to 50% of the Fe in the sample (Figure 4D). In this sample, approximately 10% of the Fe belongs to a doublet with  $\Delta E_Q \approx 2.30$  mm/s and  $\delta \approx 1.10$  mm/s (blue line in Figure 4D); this ferrous species is possibly another intermediate (tentative H200N<sub>Int2</sub><sup>HPCA</sup>, Table 2). Figure 4E shows a spectrum of a sample frozen (not by RFQ) at 180 s, a time where solution kinetics predict product will have formed and dissociated (Figure S2). However, the parameters of the observed doublet are  $\Delta E_Q = 3.10$  mm/s and  $\delta = 1.20$  mm/s (> 90% of Fe), which are slightly different than those of the substrate-free enzyme. It is possible that the high concentration of product present in the Mössbauer sample prevents net product dissociation or leads to a mixture of product bound and free enzyme in this sample. Accordingly, this species is also present in the 400 ms sample (representing roughly 20% of Fe over and above the splashed material), a time at which approximately 25 % of the enzyme is expected to be present in the product complex (Figure S2). The product proved to be insufficiently stable to make an enzyme-product complex by adding purified product to resting enzyme.

Figure 4F shows a zero field spectrum from a different set of experiments for a sample quenched at 40 ms. The sample contains ca. 70 % of the Fe in H200N<sub>Int1</sub><sup>HPCA</sup> (red line). Figure 5 shows spectra of this sample taken in parallel applied fields of 4.0 T and 8.0 T. The features observed are typical of high-spin Fe<sup>III</sup> sites (the middle section of the spectra is contaminated by the unknown spectral features of the “splashed” ferrous species). We have analyzed the spectra of H200N<sub>Int1</sub><sup>HPCA</sup> with the spin Hamiltonian  $\mathcal{H} = \mathcal{H}_e + \mathcal{H}_{hf}$  (omitting the dipole-dipole term in  $\mathcal{H}_e$  of eq 1) where  $\mathcal{H}_{hf}$  describes the <sup>57</sup>Fe hyperfine interactions.

$$\mathcal{H}_{hf} = A_0 \mathbf{S}_1 \bullet \mathbf{I}_1 + (eQV_{zz}/12) [3I^2_{1z} - 15/4 + \eta(I^2_{1x} - I^2_{1y})] - g_n \beta_n B \bullet \mathbf{I}_1 \quad [3]$$

In eq 3 all symbols have their conventional meanings. For the <sup>57</sup>Fe magnetic hyperfine coupling constant of the ferric ion, we obtained  $A_0/g_n\beta_n = -21.5 \pm 0.2$  T, which compares well with  $A_0$  values reported for octahedral Fe<sup>III</sup> sites with N/O coordination.<sup>25</sup> This observation, together with the observation that the  $\delta$  value of H200N<sub>Int1</sub><sup>HPCA</sup> falls squarely into the center of high-spin ferric  $\delta$  values, indicates that the iron is Fe<sup>III</sup> with little delocalization between the radical and the ferric ion. From the field dependence of the Mössbauer spectra, we were able to constrain the zero field splitting parameter,  $D_1$ , as follows. The observation of the resonance at  $g = 8.2$  implies that the EPR active doublet is split in zero field by  $\Delta = (4/3) 3D (E_1/D_1)^2 \approx 0.065$  cm<sup>-1</sup>; (4/3 is a spin projection factor that enters through consideration of exchange coupling when the EPR data are described by eq 2). The high field Mössbauer spectra then constrain  $D_1$  and  $(E/D)_1$  to the reasonably narrow ranges  $1.1$  cm<sup>-1</sup>  $\leq D_1 \leq 1.4$  cm<sup>-1</sup> and  $0.12 \leq (E/D)_1 \leq 0.14$ . The red lines in Figure 5 are spectral simulations of H200N<sub>Int1</sub><sup>HPCA</sup> using the parameters listed in Table 1.

**<sup>17</sup>O-Hyperfine Coupling Suggests that H200N<sub>Int1</sub><sup>HPCA</sup> Contains an Fe-Peroxo and a Substrate Radical Moiety**—To further probe the nature of the  $S = 1/2$  species in H200N<sub>Int1</sub><sup>HPCA</sup>, we have prepared samples enriched with <sup>17</sup>O in either <sup>17</sup>O<sub>2</sub> or in <sup>17</sup>O-C3-

HPCA ( $^{17}\text{O}$ ,  $I_{17\text{O}} = 5/2$ ). Parallel-mode EPR spectra of  $\text{H}_2\text{O}_2\text{N}_{\text{Int}1}^{\text{HPCA}}$  prepared with  $^{16}\text{O}_2$  (red), 70% enriched  $^{17}\text{O}_2$  (blue), and 68% enriched  $^{17}\text{O}-\text{C}_3\text{-HPCA}$  (green) are shown in Figure 6. The  $g = 8.2$  resonance of both enriched samples is broadened relative to its  $^{16}\text{O}$  counterpart. For the two samples, the broadening is the same within the experimental uncertainty.

For our analysis of the  $^{17}\text{O}$  broadenings, we used the  $S = 2$  Hamiltonian of eq 2. As will emerge shortly, the uncoupled representation of eq 1 is less suitable for this analysis. Using eq 2, SpinCount analysis yielded  $|A_z^{O,c}| = 17$  MHz for both the  $^{17}\text{O}_2$  and  $^{17}\text{O}-\text{C}_3\text{-HPCA}$  enriched samples. As mentioned above, the  $^{17}\text{O}_2$  analysis assumes that only one  $^{17}\text{O}$  nucleus contributes to the signal. The  $g = 8.2$  resonance is observed when the applied field,  $B$ , is along the molecular z-direction defined by the zero-field splitting term of eq 2. Therefore, the spectra are only sensitive to  $A_z^O$ . We have considered whether the  $^{17}\text{O}$  is part of the radical moiety (such as a superoxo radical) or whether it is part of a non-radical bearing ligand coordinated to the iron. In the former case, the  $^{17}\text{O}$  A-tensor of the coupled representation is related to the intrinsic (uncoupled) hyperfine tensor by  $\mathbf{A}^{O,c} = (-1/6)\mathbf{A}^O$ , which yields  $A_z^O = 102$  MHz. In previous work, we have characterized a related intermediate species from the same mutant HPCD using 4NC as a substrate, identified as an Fe(III)-superoxide species.<sup>19</sup> The superoxo-based radical had a substantially larger  $A_z^O = 180$  MHz, resulting in a profound broadening of the EPR signal, and different values of  $J$ ,  $D_1$  and  $(E/D)_1$  (see Table 1). One might suspect that the reduced  $A_z^O$  reflects a superoxo radical that has donated significant negative spin density to the iron. However, if this were the case, we would have observed a larger Mössbauer isomer shift and the  $^{57}\text{Fe}$  A-tensor would exhibit substantial anisotropy due to a spin-dipolar term that would reflect the ferrous admixture to the site. This consideration is in marked contrast to what is observed here. We thus conclude that  $\text{H}_2\text{O}_2\text{N}_{\text{Int}1}^{\text{HPCA}}$  does not contain a superoxo radical, but instead contains a radical which resides on the HPCA moiety, presumably as an aromatic radical. Indeed, none of the other iron ligands are likely radical sites. The broadening from  $^{17}\text{O}_2$  enrichment is therefore likely due to a peroxy species bound to the iron in a  $\text{HPCA}^\bullet\text{-Fe}^{\text{III}}\text{-(hydro)peroxy}$  complex. If the radical is located on the HPCA, the observed  $^{17}\text{O}$  hyperfine coupling would be due to covalent spin polarization delocalization of the peroxy moiety by the ferric ion. In this case, the  $^{17}\text{O}$  A-tensor in the coupled representation is related to the intrinsic (uncoupled) hyperfine tensor by  $\mathbf{A}^{O,c} = (7/6)\mathbf{A}^O$ , from which we obtain  $|A_z^O| = 15$  MHz.

The labeling of the  $^{17}\text{O}-\text{C}_3\text{-HPCA}$  results in a broadening of the spectrum comparable to that of the  $^{17}\text{O}_2$  sample. The interpretation of the broadening for  $^{17}\text{O}-\text{C}_3\text{-HPCA}$  is significantly more complex, because the C3 oxygen may have spin density contributions not only from coordination to the  $\text{Fe}^{\text{III}}$  but also from the HPCA radical. A covalent spin polarization contribution to the  $^{17}\text{O}$  hyperfine interaction induced by the  $\text{Fe}^{\text{III}}$  has a favorable spin projection factor (+7/6), compared to the (-1/6) factor for the case in which the radical resides on the HPCA moiety (N.B. The use of eq 1, rather than eq 2, would bias the primary analysis of the EPR spectra.). Thus, for comparable spin density contributions to the labeled  $\text{O}_2$  ( $\text{Fe}$  vs.  $\text{HPCA}^\bullet$ ) the A-value would be dominated by the contribution from the  $\text{Fe}^{\text{III}}$ . In the absence of quantitative insight about the source of the spin density at the C3 oxygen by quantum chemical calculations it seems prudent to reserve judgment as to the precise origin of the broadening by  $^{17}\text{O}-\text{C}_3\text{-HPCA}$ . (footnote 3)

---

<sup>3</sup>Very little EPR linewidth change was observed when uniformly enriched  $^{13}\text{C}$ -HPCA was used (data not shown). Since the  $^{13}\text{C}$  would be part of the radical moiety, the spin projection factor (-1/6) would strongly suppress the broadening. Ongoing DFT computations showed that the  $^{13}\text{C}$  enrichment would not broaden the  $g = 8.2$  resonance to any significant extent even if the radical would be centered on labeled carbon.

## Stopped-flow Spectroscopy of the FeHPCA + O<sub>2</sub> Reaction Reveals No Evidence for an Intermediate Similar to H200N<sub>Int1</sub><sup>HPCA</sup>

Figure 7 shows diode spectra from the single-turnover reaction in which pre-formed, anaerobic, stoichiometric FeHPCD-HPCA substrate complex is rapidly mixed with O<sub>2</sub>-containing buffer at 4 °C. The spectra show only formation of the ring-cleaved product with  $\lambda_{\text{max}}$  near 380 nm with no detectable chromophore in the lower energy region from 500 - 700 nm; reaction of a 1 mM FeHPCD-HPCA sample also failed to show a long wavelength band. However, kinetic analysis of product formation using a single wavelength trace at 380 nm has previously revealed that product formation proceeds in several phases, including a fast phase that decays with  $k_1 \sim 38 \text{ s}^{-1}$  and a slower phase with  $k_2 \sim 3.8 \text{ s}^{-1}$ .<sup>20</sup>

In our current preparations, both rates are slightly faster ( $k_1 = 59 \pm 4 \text{ s}^{-1}$  and with  $k_2 = 6.0 \pm 0.5 \text{ s}^{-1}$ ). The fast phase is associated with a lag in product formation as shown in Figure 7, *inset*, and precedes formation of the product chromophore. Consequently, while there are discrete intermediates in the oxygen activation and insertion processes, none of the detectable intermediates have optical features like H200N<sub>Int1</sub><sup>HPCA</sup>. Following mixing of the FeHPCD-HPCA complex with O<sub>2</sub>, single wavelength data at 380 nm (Figure 7, *inset*) show that the lag phase persists to ~ 30 ms, providing an opportunity to use the RFQ approach for trapping reaction intermediates that precede product formation in the FeHPCD + O<sub>2</sub> reaction.

## RFQ Samples from the FeHPCD + O<sub>2</sub> Reaction Reveal an Fe<sup>II</sup> Reaction Intermediate

Because both the H200N-4NC + O<sub>2</sub> and H200N-HPCA + O<sub>2</sub> reactions have revealed high yields of oxygenated intermediates at times < 1 s (Figure 1-6<sup>19</sup>), we have prepared RFQ samples from the WT FeHPCD-HPCA + O<sub>2</sub> reaction in order to look for reaction intermediates associated with the lag phase in the kinetic time course before product formation.

The Mössbauer spectrum of the resting state WT enzyme consists of one doublet with  $\Delta E_Q = 2.97 \text{ mm/s}$  and  $\delta = 1.23 \text{ mm/s}$ , consistent with a 6-coordinate high-spin Fe<sup>II</sup> species (Figure 8A).<sup>2,23</sup> Anaerobic addition of HPCA to the resting state WT enzyme yields a Mössbauer spectrum consisting of two ferrous doublets (Figure 8B). One doublet accounts for 55% of the iron with parameters  $\Delta E_Q = 3.29 \text{ mm/s}$  and  $\delta = 1.14 \text{ mm/s}$  (FeHPCD<sub>ES1</sub><sup>HPCA</sup>, Table 2) while the other species has 45% of the iron giving a doublet with parameters  $\Delta E_Q = 2.18 \text{ mm/s}$  and  $\delta = 1.18 \text{ mm/s}$  (FeHPCD<sub>ES2</sub><sup>HPCA</sup>, Table 2) (footnote 2). Note that these parameters differ from those observed for the H200N-HPCA complex. The spectrum of a sample frozen at 15 ms, which is within the lag phase of the FeHPCD-HPCA + O<sub>2</sub> reaction, is shown in Figure 8C. It reveals two new species exhibiting quadrupole doublets from ferrous ions. One doublet has  $\Delta E_Q = 2.33 \text{ mm/s}$ ,  $\delta = 1.08 \text{ mm/s}$  (FeHPCD<sub>Int1</sub><sup>HPCA</sup>, Table 2) and accounts for ~ 70% of the iron. This species appears to decay to the second species which has parameters similar to those of the resting state enzyme ( $\Delta E_Q = 3.03 \text{ mm/s}$ ,  $\delta = 1.24 \text{ mm/s}$ ) (Figure 8D). This second species amounts to ~ 95% of the signal shown at the end of the reaction (Figure 8E). It is not clear whether this is the product-free resting enzyme or enzyme with product still bound due to its relatively high concentration in the Mössbauer sample. Its presence in the 15 ms sample may again be due to splash from the freezing wheels at high ram velocity. Our combined stopped-flow and RFQ/Mössbauer data suggest that FeHPCD<sub>Int1</sub><sup>HPCA</sup> is a ferrous reaction intermediate which accumulates to nearly quantitative yields in the reaction cycle of the WT enzyme.

## DISCUSSION

The isolation and characterization of the intermediates that follow binding of O<sub>2</sub> in the reaction cycle of Fe<sup>II</sup>-containing catechol dioxygenases such as FeHPCD has been an elusive goal. Our recent characterization of the relatively long-lived intermediates in the reaction of H200N-4NC with O<sub>2</sub> was informative; however, the reaction leads to ring oxidation rather than ring cleavage.<sup>18,19</sup> The short lifetimes of intermediates in the reaction cycles of WT and mutant enzymes catalyzing ring cleavage reactions present a greater challenge. Here, the intermediates formed after oxygen binding in the H200N- and FeHPCD-catalyzed ring cleavage of HPCA have been trapped for spectroscopic characterization and comparison. The results show that the first intermediates trapped after O<sub>2</sub> addition in each of these systems differ fundamentally from each other as well as from the 4NC-Fe<sup>III</sup>-superoxide intermediate trapped in the non-ring cleaving H200N-4NC + O<sub>2</sub> system. The structural insights gained from the evaluation of the spectra of these intermediates and the relevance to the mechanism of O<sub>2</sub> activation for aromatic ring cleavage are discussed here.

### Identity of H200N<sub>Int1</sub><sup>HPCA</sup>

The studies described here show that H200N<sub>Int1</sub><sup>HPCA</sup> contains a high-spin Fe<sup>III</sup> ( $S_I = 5/2$ ) site that is antiferromagnetically coupled to a radical ( $S_R = 1/2$ ) to yield a ground multiplet with  $S = 2$ . The <sup>57</sup>Fe magnetic hyperfine coupling of H200N<sub>Int1</sub><sup>HPCA</sup> ( $A_0/g_n\beta_n = -21.5$  T) compares well to those observed for mononuclear Fe<sup>III</sup> sites and the isomer shift,  $\delta = 0.48$  mm/s, is characteristic of octahedral high-spin Fe<sup>III</sup> sites with N/O ligands (Table 1).<sup>2,19,23,26</sup> As judged by the values of  $A_0$  and  $\delta$ , one electron has been transferred from the Fe<sup>II</sup>. A radical species that couples to the resulting Fe<sup>III</sup> must have been formed either directly or indirectly as a result of this transfer.

The most likely candidates for the  $S_R = 1/2$  species bound to the Fe<sup>III</sup> are suggested by the two intermediates discovered during our previous study of the H200N-4NC + O<sub>2</sub> reaction; namely, H200N<sub>Int1</sub><sup>4NC</sup> formulated as 4NC-Fe<sup>III</sup>-O<sub>2</sub><sup>•-</sup> and H200N<sub>Int2</sub><sup>4NC</sup> formulated as 4NC<sup>•-</sup>-Fe<sup>III</sup>-(hydro)peroxo. The spectroscopic data for H200N<sub>Int1</sub><sup>HPCA</sup> are overall quite similar to those of the latter, H200N<sub>Int2</sub><sup>4NC</sup>, and differ significantly from the former. Specific similarities include: Mössbauer parameters, EPR spectra, substantial positive  $J$  values (antiferromagnetic) with  $D_1 > 0$ , and small <sup>17</sup>O hyperfine constants. In contrast, the 4NC-Fe<sup>III</sup>-O<sub>2</sub><sup>•-</sup> complex has much smaller  $J$  value (6 cm<sup>-1</sup>),  $D_1 < 0$ , and its EPR signal is significantly more broadened when <sup>17</sup>O<sub>2</sub> is used. Thus, we propose that H200N<sub>Int1</sub><sup>HPCA</sup> is formulated as HPCA<sup>•-</sup>-Fe<sup>III</sup>-(hydro)peroxo. (footnote 3)

The HPCA-SQ<sup>•</sup> as the site of the radical is in accord with the crystallographic structure of the oxy-intermediate formed in the reaction of FeHPCD-4NC with O<sub>2</sub>, which revealed substantial ring deformation at the carbon where oxygen subsequently attacks to form the alkylperoxo intermediate. This suggests that a localized radical forms at this carbon of the ring.<sup>12</sup> However, the 2.4 Å bond lengths of the metal ligands to the bound dioxygen species which we see in this intermediate suggest that the iron is in the Fe<sup>II</sup> state. This would mean that the bound oxygen is likely to be superoxo rather than peroxo.

The UV-vis spectrum of H200N<sub>Int1</sub><sup>HPCA</sup> shows three main features; namely, a high energy shoulder at ~310 nm ( $\epsilon_{310\text{ nm}} \sim 7000\text{ M}^{-1}\text{ cm}^{-1}$ ), a maximum at 395 nm ( $\epsilon_{395\text{ nm}} \sim 3200\text{ M}^{-1}\text{ cm}^{-1}$ ) and a lower energy feature near 610 nm ( $\epsilon_{610\text{ nm}} \sim 1100\text{ M}^{-1}\text{ cm}^{-1}$ ). This spectrum is inconsistent with HPCA bound in the catecholic form.<sup>27-29</sup> The two higher energy features are similar to those observed for unbound catechol quinones and semiquinones, which themselves have similar spectra (Table S2).<sup>30,31</sup> Indeed, the spectrum of H200N<sub>Int1</sub><sup>HPCA</sup> in the 300-500 nm region is very similar to that of HPCA quinone (Figure 1A, *inset*, blue

dashed spectrum). Binding of these molecules to oxidized metals causes little change in the band positions or intensities. However, the semiquinone complexes can give rise to additional charge transfer bands in the 600 - 800 nm region with widely ranging extinction coefficients (300 - 3000 M<sup>-1</sup> cm<sup>-1</sup>) (Table S2).<sup>32,33</sup> Very few ligand-Fe<sup>III</sup>-SQ<sup>•</sup> model complexes with  $S = 2$  have been spectroscopically characterized, but those available show similar optical characteristics (Table S2).<sup>33-35</sup> When considered in light of the EPR and Mössbauer analysis, the optical spectrum of H200N<sub>Int1</sub><sup>HPCA</sup> is most consistent with a HPCA-SQ<sup>•</sup> radical and peroxy ligands bound to Fe<sup>III</sup>.

While the 610 nm chromophore may derive from an HPCA SQ<sup>•</sup>-Fe<sup>III</sup> interaction, another possibility is a (hydro)peroxy-to-Fe<sup>III</sup> LMCT band, given the structure of H200N<sub>Int1</sub><sup>HPCA</sup> proposed here. A band in this region might also arise from a Fe<sup>III</sup>-OOR complex, but in the current case, this would be the alkylperoxy intermediate of the reaction cycle which is expected to contain Fe<sup>II</sup> based on computational studies.<sup>36,37</sup> Many end-on Fe<sup>III</sup>-OOH and side-on bound Fe<sup>III</sup>-O<sub>2</sub><sup>2-</sup> complexes from non-heme mononuclear model complexes have been characterized (Table S2).<sup>38,39</sup> The Fe<sup>III</sup>-OOH complexes are often low-spin when the iron is coordinated by nitrogen ligands, but incorporation of at least one carboxylate ligand can result in a high spin Fe<sup>III</sup>-OOH complex as would pertain to the intermediates of FeHPCD. In comparison to the 610 nm species observed here, the high spin Fe<sup>III</sup>-OOH model complexes generally have a UV-vis transition with comparable intensity ( $\epsilon = 450 - 2000$  M<sup>-1</sup> cm<sup>-1</sup>) but shorter  $\lambda_{\text{max}}$  (440 - 570 nm) (Table S2).<sup>38,39</sup>

In model compounds, it has been shown that the Fe<sup>III</sup>-OOH complexes can be deprotonated to form the conjugate base side-on bound Fe<sup>III</sup>-O<sub>2</sub><sup>2-</sup> complex for pH > 10.<sup>38,39</sup> In such a case, the resultant complex is often high spin, exhibiting a  $\lambda_{\text{max}}$  shift into the range of the 610 nm species ( $\lambda_{\text{max}} \sim 525 - 750$  nm), but the  $\epsilon$  values ( $\epsilon = 450 - 600$  M<sup>-1</sup> cm<sup>-1</sup>) are lower. Many of these side-on peroxy species have an EPR spectrum originating from an excited state like H200N<sub>Int1</sub><sup>HPCA</sup>, but the Mössbauer isomer shift is somewhat larger (0.66 mm/s vs 0.48 mm/s). A third possibility is suggested by the high spin Fe<sup>III</sup>-(hydro)peroxy intermediate in benzoate 1,2-dioxygenase, which we know from the crystal structure of the equivalent intermediate found in naphthalene 1,2-dioxygenase to be a side-on bound Fe<sup>III</sup> species.<sup>40</sup> Our spectroscopic analysis of the species from benzoate 1,2 dioxygenase shows that the Mössbauer isomer shift is 0.5 mm/s, as found for H200N<sub>Int1</sub><sup>HPCA</sup>. We have proposed that this is due to protonation of the side-on bound peroxy moiety.<sup>41</sup> If this is the case, a pH dependence might be expected for the low energy band of the H200N<sub>Int1</sub><sup>HPCA</sup> spectrum, but none is observed in the range between pH 5.5 and 9.0 (Figure 1B, *inset*). One possible explanation for this is that the  $pK_a$  for this type of species is relatively high, as observed for the end-on hydroperoxo complexes, such that it remains protonated throughout the range of stability for the enzyme. Based on this analysis, it is not currently possible to definitively assign the origin of the 610 nm species, and it could, in fact, result from the sum of both Fe<sup>III</sup>-HPCA SQ<sup>•</sup> and Fe<sup>III</sup>-(hydro)peroxy interactions.

### Identity of H200N<sub>Int2</sub><sup>HPCA</sup>

Analysis of transient kinetic data from the time course of the 610 nm intermediate as well as product formation in the H200N-HPCA + O<sub>2</sub> reaction (values from the current preparation are shown in Figure S1, S2 and Scheme 2)<sup>18</sup> suggests that H200N<sub>Int1</sub><sup>HPCA</sup> accumulates to near stoichiometric yield. This is in accord with the Mössbauer and EPR spectra of this reaction intermediate shown here. On the other hand, the kinetic model predicts H200N<sub>Int2</sub><sup>HPCA</sup> would accumulate to only ~12 % at 400 ms due to the rapid decay of the species (Figure S2). Analysis of the Mössbauer reaction time-course does show that H200N<sub>Int2</sub><sup>HPCA</sup> accumulates to only ~10 % at 400 ms (Figure 6C). Due to low yields of H200N<sub>Int2</sub><sup>HPCA</sup>, we were unable to obtain precise Mössbauer parameters of this species. However, it is clear that H200N<sub>Int2</sub><sup>HPCA</sup> is ferrous with  $\Delta E_Q \approx 2.33$  mm/s and  $\delta \approx 1.1-1.2$

mm/s. It is possible that this species is either the predicted (Scheme 1D) HPCA<sup>•</sup>-Fe<sup>II</sup>-O<sub>2</sub><sup>•</sup>, or perhaps more likely, the Fe<sup>II</sup>-alkylperoxo or lactone intermediates, which derive from H200N<sub>Int1</sub><sup>HPCA</sup> prior to formation of the yellow ring cleaved product.

### Identity of FeHPCD<sub>Int1</sub><sup>HPCA</sup>

The Mössbauer parameters for FeHPCD<sub>Int1</sub><sup>HPCA</sup> show that this reaction intermediate contains a high-spin Fe<sup>II</sup> site, in sharp contrast to the Fe<sup>III</sup> containing initial intermediates described here and in our earlier study.<sup>19</sup> Unlike H200N<sub>Int1</sub><sup>HPCA</sup>, no optical spectrum of this intermediate could be detected even in the first few milliseconds of the reaction. Consequently, our stopped-flow studies of the FeHPCD-HPCA + O<sub>2</sub> reaction were limited to monitoring product formation, which is clearly at least a two step process.<sup>20</sup> The largest reciprocal relaxation time from this process makes the largest contribution to the observed lag phase and shows no O<sub>2</sub> concentration dependence. Thus, it is dominated by the rate constants for a step separated from the initial O<sub>2</sub> binding by at least one irreversible step. FeHPCD<sub>Int1</sub><sup>HPCA</sup> is temporally associated with this initial lag in product formation, suggesting that it occurs after the effectively irreversible step in the reaction. The lack of an optical spectrum from a semiquinone or quinone for FeHPCD<sub>Int1</sub><sup>HPCA</sup> is consistent with this hypothesis and also argues against a HPCA SQ<sup>•</sup>-Fe<sup>II</sup>-O<sub>2</sub><sup>•</sup> or HPCA quinone-Fe<sup>II</sup>-(hydro)peroxo structure. FeHPCD<sub>Int1</sub><sup>HPCA</sup> cannot be a product complex which would be intensely yellow even before dissociation from the enzyme; the true product complex builds on a much longer time scale. Taken together, these observations suggest FeHPCD<sub>Int1</sub><sup>HPCA</sup> is one of the intermediates that results after oxygen attacks the substrate, but before ring cleavage, such as the alkylperoxo or lactone intermediates of the proposed reaction cycle. Accordingly, the Mössbauer parameters for this species are very similar to those of H200N<sub>Int2</sub><sup>HPCA</sup> which is postulated above to be such a species.

### Mechanistic Implications of the Observed Intermediates

Our studies of the intermediates of the O<sub>2</sub> activation and insertion portion of the extradiol dioxygenase reaction cycle have shown that the nature and reactivity of the intermediates are functions of both the electronic characteristics of the substrate and the amino acid residues present in the second sphere of the active site. Scheme 3 illustrates the intermediates that have been trapped and characterized by various means. Studies thus far have focused on substrates with progressively more electron withdrawing *para*-substituents and mutation of the key acid/base catalyst, His200. It is found that when a shorter Asn residue is substituted for His200, two types of intermediates can rapidly form in nearly 100% yield, both of which contain Fe<sup>III</sup> spin-coupled to a radical. More specifically, an end-on bound Fe<sup>III</sup>-O<sub>2</sub><sup>•</sup> adduct is formed when the substrate has a strongly electron withdrawing *p*-nitro substituent (Scheme 3B),<sup>19</sup> whereas a substrate SQ<sup>•</sup>-Fe<sup>III</sup>-(hydro)peroxo species (peroxo orientation is not definitively determined) is formed when HPCA with its electron donating substituent is used (Scheme 3C). These two intermediates differ substantially not only in their respective lifetimes, but also in the eventual outcomes of catalysis.

The 4NC-Fe<sup>III</sup>-O<sub>2</sub><sup>•</sup> intermediate persists for many minutes and eventually yields 4NC-quinone and H<sub>2</sub>O<sub>2</sub>, whereas the HPCA SQ<sup>•</sup>-Fe<sup>III</sup>-(hydro)peroxo intermediate disappears in 2 s at 4 °C and yields the normal ring cleaved product. The ability of O<sub>2</sub> to bind to the enzyme is also affected by the *para*-substituent of the substrate in the H200N mutant such that the binding rate constant is 4-fold slower and the reaction becomes reversible when 4NC is bound in place of HPCA.<sup>18</sup> These observations suggest that the effects of either electron withdrawal or donation in the substrate ring are transmitted through the iron to affect its ability to share electrons with the O<sub>2</sub> during binding. We have proposed that this transmission of electron density from the substrate through the iron to the bound O<sub>2</sub> is a fundamental aspect of oxygen activation in this enzyme family.<sup>10,12,13</sup>

The reaction of the native enzyme with 4NC and HPCA reveals other aspects of the mechanism. When His200 is present, substrates with either electron withdrawing or donating substituents are converted into ring-cleaved products, albeit at 25-fold different rates. The crystallographically characterized intermediate in the reaction of FeHPCD-4NC with O<sub>2</sub> (FeHPCD<sub>Int1</sub><sup>4NC</sup>) (Scheme 3D)<sup>12</sup> and the spectroscopically characterized FeHPCD<sub>Int1</sub><sup>HPCA</sup> intermediate (Scheme 3E) described here both have Fe<sup>II</sup> in the active site rather than Fe<sup>III</sup>. However, the former appears to be a species with radical character on both the substrate and the bound O<sub>2</sub>, while it is argued above that the latter is likely to be a state after oxygen attack on the substrate. If this is the case, then the formation and reaction of the reactive oxygen intermediate(s) must be very fast such that there is no evidence for any of the types of spin-coupled Fe<sup>III</sup> intermediates described here or in our previous study. This may mean that an Fe<sup>III</sup> species of some sort forms, but its lifetime is too short to be detected even on the millisecond time scale. Alternatively, the iron may serve purely as a conduit for electron density that does not change oxidation state as an electron is transferred from the catechol to O<sub>2</sub>. The final alternative, namely that there is no transfer of electron density between the substrates, is unlikely because the reaction of unactivated oxygen with catechols is slow and does not result in ring cleavage.

## Conclusion

The oxy-intermediates that have been trapped thus far using FeHPCD and its variants with HPCA and alternative substrates show that a radical species can reside on either the substrate or the oxygen and that an electron can be transferred from the iron, the substrate, or both to the oxygen. Based on the *in crystallo* studies published previously,<sup>12</sup> it is possible for an electron to be transferred in either a stepwise or a concerted fashion from the iron to the oxygen and from the substrate to the iron to yield a diradical pair. All of these observations support the most fundamental aspect of catalysis established for this enzyme class which envisions oxygen activation by coordinating oxygen reduction with substrate oxidation to form a reactive pair. The results reported in our previous study show that simple formation of an Fe<sup>III</sup>-O<sub>2</sub><sup>•-</sup> species alone is not sufficient for high reactivity or ring cleaving chemistry. The current study suggests that, following electron transfer from the substrate, either a substrate SQ<sup>•</sup>-Fe<sup>II</sup>-O<sub>2</sub><sup>•-</sup> or a substrate SQ<sup>•</sup>-Fe<sup>III</sup>-peroxo intermediate might serve as the reactive species. However, the high reactivity of the enzyme containing Fe<sup>II</sup>, Mn<sup>II</sup>, or Co<sup>II</sup><sup>15,16</sup> favors the substrate SQ<sup>•</sup>-Fe<sup>II</sup>-O<sub>2</sub><sup>•-</sup> species, for which there is no net change in oxidation state between the enzyme-substrate complex and the reactive species. Although the current study suggests for the first time that a substrate SQ<sup>•</sup>-Fe<sup>III</sup>-peroxo intermediate can lead to ring cleavage, its low rate of reaction suggests that it is not the species that carries out this reaction in the reaction cycle of the WT enzyme. It is notable that the maximum rate of O<sub>2</sub> activation and reaction is only achieved when His200 is present. This is consistent with our previous proposal that this residue plays many roles over and above its role as an acid base catalyst.<sup>18</sup> These may include charge stabilization that promotes formation of the SQ-Fe<sup>II</sup>-O<sub>2</sub><sup>•-</sup> species as well as hydrogen bonding and steric interactions that properly orient the superoxo species for reaction with the activated substrate.

## Supplementary Material

Refer to Web version on PubMed Central for supplementary material.

## Acknowledgments

We would like to thank Dr. David P. Ballou for the generous gift of the C1 and C2 enzymes used for synthesis of <sup>17</sup>O-labeled HPCA.

### Funding Sources

This work is supported by the NIH grant GM 24689 (to J. D. L.), grant EB-001475 (to E.M.), grant GM77387 (to M. P. H.) and graduate traineeship GM08700 (to M. M. M.).

## ABBREVIATIONS

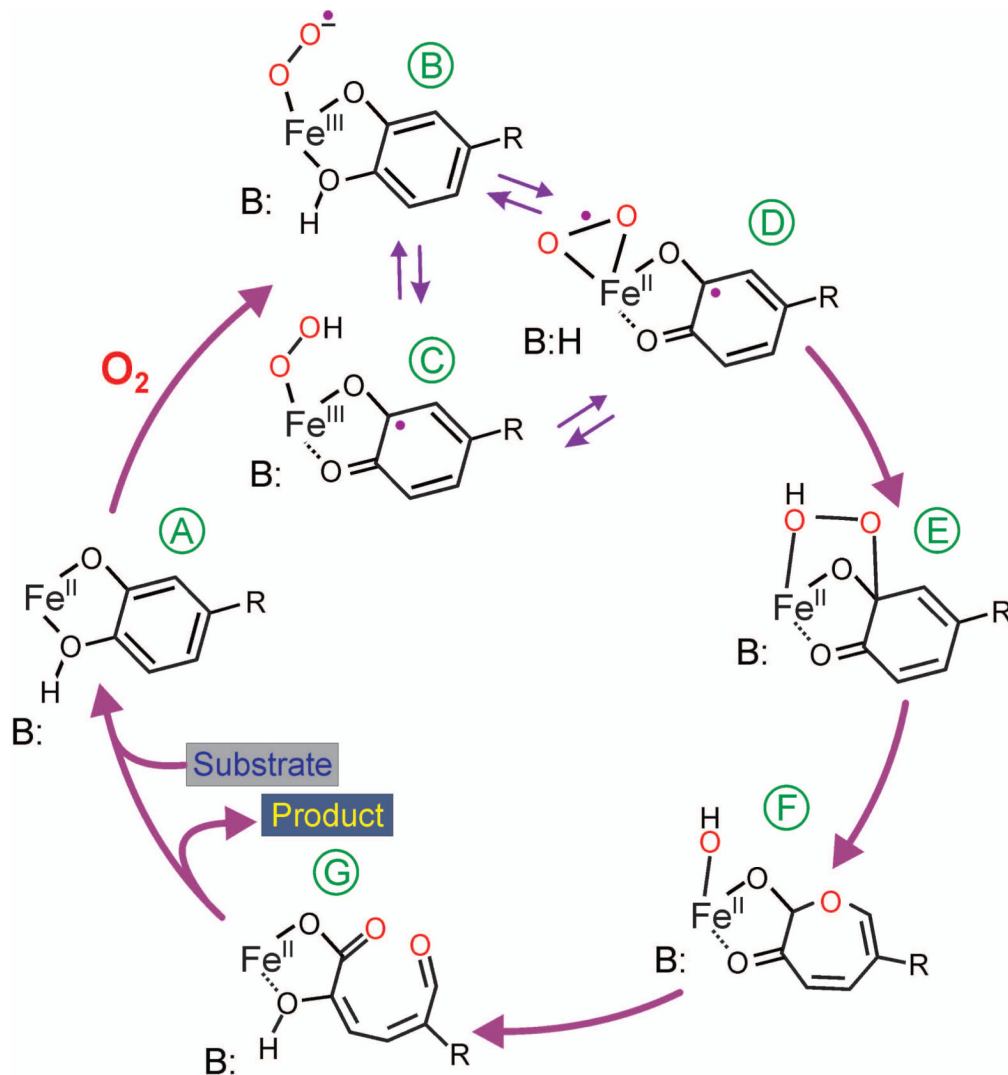
<b>FeHPCD</b>	recombinant homoprotocatechuate 2,3-dioxygenase from <i>Brevibacterium fuscum</i>
<b>MnHPCD</b>	recombinant homoprotocatechuate 2,3-dioxygenase from <i>Brevibacterium fuscum</i> in which the Fe <sup>II</sup> is replaced by Mn <sup>II</sup>
<b>H200N</b>	His to Asn variant of FeHPCD at position 200
<b>HPCA</b>	homoprotocatechuate or 3,4 dihydroxyphenylacetate
<b>4NC</b>	4-nitrocatechol
<b>WT</b>	wild type
<b>RFQ</b>	rapid freeze quench
<b>SQ<sup>•</sup></b>	semiquinone radical
<b>H200N<sub>Int1</sub><sup>4NC</sup></b>	the spin coupled high-spin 4NC-Fe <sup>III</sup> -superoxo complex of H200N
<b>H200N<sub>Int2</sub><sup>4NC</sup></b>	the spin coupled high-spin 4NC SQ <sup>•</sup> -Fe <sup>III</sup> -(hydro)peroxy complex of H200N
<b>H200N<sub>Int1</sub><sup>HPCA</sup> and H200N<sub>Int2</sub><sup>HPCA</sup></b>	intermediates observed in the H200N-HPCA + O <sub>2</sub> reaction
<b>FeHPCD<sub>Int1</sub><sup>HPCA</sup></b>	intermediate observed in the FeHPCD-HPCA + O <sub>2</sub> reaction
<b>H200N<sub>ES1</sub><sup>HPCA</sup>, H200N<sub>ES2</sub><sup>HPCA</sup>, FeHPCD<sub>ES1</sub><sup>HPCA</sup>, and FeHPCD<sub>ES2</sub><sup>HPCA</sup></b>	substrate complexes of H200N or FeHPCD with the substrate HPCA
<b>EPR</b>	electron paramagnetic resonance
<b>LMCT</b>	ligand to metal charge transfer transition

## REFERENCES

- Lipscomb JD, Orville AM. Mechanistic aspects of dihydroxybenzoate dioxygenases. Metal Ions Biol. Syst. 1992; 28:243–298.
- Arciero DM, Lipscomb JD, Huynh BH, Kent TA, Münck E. EPR and Mössbauer studies of protocatechuate 4,5-dioxygenase. Characterization of a new Fe<sup>2+</sup> environment. J. Biol. Chem. 1983; 258:14981–14991. [PubMed: 6317682]
- Boldt YR, Sadowsky MJ, Ellis LBM, Que L, Wackett LP. A manganese-dependent dioxygenase From *Arthrobacter globiformis* CM-2 belongs to the major extradiol dioxygenase family. J. Bacteriol. 1995; 177:1225–1232. [PubMed: 7868595]
- Vaillancourt FH, Bolin JT, Eltis LD. The ins and outs of ring-cleaving dioxygenases. Crit. Rev. Biochem. Mol. Biol. 2006; 41:241–267. [PubMed: 16849108]
- Kovaleva EG, Neibergall MB, Chakrabarty S, Lipscomb JD. Finding intermediates in the O<sub>2</sub> activation pathways of non-heme iron oxygenases. Acc. Chem. Res. 2007; 40:475–483. [PubMed: 17567087]
- Dagley S. Microbial catabolism, the carbon cycle and environmental pollution. Die Naturwissenschaften. 1978; 65:85–95. [PubMed: 345130]

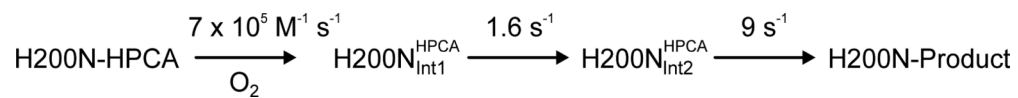
7. Bugg TDH, Winfield CJ. Enzymic cleavage of aromatic rings: mechanistic aspects of the catechol dioxygenases and later enzymes of bacterial oxidative cleavage pathways. *Nat. Prod. Rep.* 1998; 15:513–530.
8. Hegg EL, Que L. The 2-His-1-carboxylate facial triad: An emerging structural motif in mononuclear non-heme iron(II) enzymes. *Eur. J. Biochem.* 1997; 250:625–629. [PubMed: 9461283]
9. Arciero DM, Orville AM, Lipscomb JD. [ $^{17}\text{O}$ ]Water and nitric oxide binding by protocatechuate 4,5-dioxygenase and catechol 2,3-dioxygenase. Evidence for binding of exogenous ligands to the active site  $\text{Fe}^{2+}$  of extradiol dioxygenases. *J. Biol. Chem.* 1985; 260:14035–14044. [PubMed: 2997190]
10. Arciero DM, Lipscomb JD. Binding of  $^{17}\text{O}$ -labeled substrate and inhibitors to protocatechuate 4,5-dioxygenase-nitrosyl complex. Evidence for direct substrate binding to the active site  $\text{Fe}^{2+}$  of extradiol dioxygenases. *J. Biol. Chem.* 1986; 261:2170–2178. [PubMed: 3003098]
11. Kovaleva EG, Lipscomb JD. Versatility of biological non-heme Fe(II) centers in oxygen activation reactions. *Nat. Chem. Biol.* 2008; 4:186–193. [PubMed: 18277980]
12. Kovaleva EG, Lipscomb JD. Crystal structures of  $\text{Fe}^{2+}$  dioxygenase superoxo, alkylperoxo, and bound product intermediates. *Science.* 2007; 316:453–457. [PubMed: 17446402]
13. Shu L, Chiou YM, Orville AM, Miller MA, Lipscomb JD, Que L Jr. X-ray absorption spectroscopic studies of the Fe(II) active site of catechol 2,3-dioxygenase. Implications for the extradiol cleavage mechanism. *Biochemistry.* 1995; 34:6649–6659. [PubMed: 7756296]
14. Spence EL, Langley GJ, Bugg TDH. Cis-trans isomerization of a cyclopropyl radical trap catalyzed by extradiol catechol dioxygenases: Evidence for a semiquinone intermediate. *J. Am. Chem. Soc.* 1996; 118:8336–8343.
15. Emerson JP, Kovaleva EG, Farquhar ER, Lipscomb JD, Que L Jr. Swapping metals in Fe- and Mn-dependent dioxygenases: Evidence for oxygen activation without a change in metal redox state. *Proc. Natl. Acad. Sci. U. S. A.* 2008; 105:7347–7352. [PubMed: 18492808]
16. Fielding AJ, Kovaleva EG, Farquhar ER, Lipscomb JD, Que L Jr. A hyperactive cobalt-substituted extradiol-cleaving catechol dioxygenase. *J. Biol. Inorg. Chem.* 2011; 16:341–355. [PubMed: 21153851]
17. Gunderson WA, Zatsman AI, Emerson JP, Farquhar ER, Que L, Lipscomb JD, Hendrich MP. Electron paramagnetic resonance detection of intermediates in the enzymatic cycle of an extradiol dioxygenase. *J. Am. Chem. Soc.* 2008; 130:14465–14467. [PubMed: 18839948]
18. Groce SL, Lipscomb JD. Aromatic ring cleavage by homoprotocatechuate 2,3-dioxygenase: Role of His200 in the kinetics of interconversion of reaction cycle intermediates. *Biochemistry.* 2005; 44:7175–7188. [PubMed: 15882056]
19. Mbughuni MM, Chakrabarti M, Hayden JA, Bominaar EL, Hendrich MP, Münck E, Lipscomb JD. Trapping and spectroscopic characterization of an FeIII-superoxide intermediate from a nonheme mononuclear iron-containing enzyme. *Proc. Natl. Acad. Sci. U. S. A.* 2010; 107:16788–16793. [PubMed: 20837547]
20. Groce SL, Miller-Rodeberg MA, Lipscomb JD. Single-turnover kinetics of homoprotocatechuate 2,3-dioxygenase. *Biochemistry.* 2004; 43:15141–15153. [PubMed: 15568806]
21. Jollie DR, Lipscomb JD. Formate dehydrogenase from *Methylosinus trichosporium* OB3b. *Methods Enzymol.* 1990; 188:331–334. [PubMed: 2126333]
22. Miller MA, Lipscomb JD. Homoprotocatechuate 2,3-dioxygenase from *Brevibacterium fuscum* - A dioxygenase with catalase activity. *J. Biol. Chem.* 1996; 271:5524–5535. [PubMed: 8621411]
23. Münck, E. Aspects of  $^{57}\text{Fe}$  Mössbauer spectroscopy. In: Que, L., Jr, editor. *Physical Methods in Bioinorganic Chemistry.* University Science Books; Sausalito, CA: 2000. p. 287-319.
24. Sucharitakul J, Chaiyen P, Entsch B, Ballou DP. The reductase of p-hydroxyphenylacetate 3-hydroxylase from *Acinetobacter baumannii* requires p-hydroxyphenylacetate for effective catalysis. *Biochemistry.* 2005; 44:10434–10442. [PubMed: 16042421]
25. Whittaker JW, Lipscomb JD, Kent TA, Münck E. *Brevibacterium fuscum* protocatechuate 3,4-dioxygenase. Purification, crystallization, and characterization. *J. Biol. Chem.* 1984; 259:4466–4475. [PubMed: 6323474]

26. Wolgel SA, Dege JE, Perkins-Olson PE, Jaurez-Garcia CH, Crawford RL, Münck E, Lipscomb JD. Purification and characterization of protocatechuate 2,3-dioxygenase from *Bacillus macerans*: A new extradiol catecholic dioxygenase. *J. Bacteriol.* 1993; 175:4414–4426. [PubMed: 8392511]
27. Costas M, Mehn M,P, Jensen M,P, Que L Jr. Dioxygen activation at mononuclear nonheme iron active sites: enzymes, models, and intermediates. *Chem. Rev.* 2004; 104:939–986. [PubMed: 14871146]
28. Cox DD, Benkovic SJ, Bloom LM, Bradley FC, Nelson MJ, Que L Jr. Wallick DE. Catecholate LMCT bands as probes for the active sites of nonheme iron oxygenases. *J. Am. Chem. Soc.* 1988; 110:2026–2032.
29. Anitha N, Palaniandavar M. Mononuclear iron(III) complexes of 3N ligands in organized assemblies: spectral and redox properties and attainment of regioselective extradiol dioxygenase activity. *J. Chem. Soc., Dalton Trans.* 2011; 40:1888–1901.
30. Stallings MD, Morrison MM, Sawyer DT. Redox chemistry of metal-catechol complexes in aprotic media. 1. Electrochemistry of substituted catechols and their oxidation products. *Inorg. Chem.* 1981; 20:2655–2660.
31. Chedekel MR, Land EJ, Thompson A, Truscott TG. Early steps in the free radical polymerization of 3,4-dihydroxyphenylalanine (dopa) into melanin. *J. Chem. Soc., Chem. Commun.* 1984:1170–1172.
32. Hartl F, Stufkens DJ, Vlcek A Jr. Nature of the manganese(I)-dioxiolene bonding as a function of the ligand oxidation state: UV-visible, IR, and resonance Raman spectroelectrochemical study of  $[\text{Mn}(\text{CO})_3\text{L}_n(\text{Diox})]^z$  ( $n = 0, 1$ ;  $z = -2, -1, 0, +1$ ) and  $[\text{Mn}(\text{CO})_2\{\text{P}(\text{OEt})_3\}_m(\text{Diox})]^z$  ( $m = 1, 2$ ;  $z = -1, 0, +1$ ) complexes. *Inorg. Chem.* 1992; 31:1687–1695.
33. Mialane P, Anxolabehermallart E, Blondin G, Nivorojkine A, Guilhem J, Tchertanova L, Cesario M, Ravi N, Bominaar E, Girerd JJ, Münck E. Structure and electronic properties of (N,N'-Bis(4-Methyl-6-Tert-Butyl-2-Methyl-Phenolate)-N,N'-bismethyl-1,2-di aminoethane)Fe-III (DBSQ) - Spectroelectrochemical study of the red-ox properties - Relevance to intradiol catechol dioxygenases. *Inorg. Chim. Acta.* 1997; 263:367–378.
34. Kessel SL, Emberson RM, Debrunner PG, Hendrickson DN. Iron(III), manganese(III), and cobalt(III) complexes with single chelating o-semiquinone ligands. *Inorg. Chem.* 1980; 19:1170–1178.
35. Lynch MW, Valentine M, Hendrickson DN. Mixed-valence semi-quinone catecholate iron complexes. *J. Am. Chem. Soc.* 1982; 104:6982–6989.
36. Siegbahn PEM, Haeffner F. Mechanism for catechol ring-cleavage by non-heme iron extradiol dioxygenases. *J. Am. Chem. Soc.* 2004; 126:8919–8932. [PubMed: 15264822]
37. Deeth RJ, Bugg TDH. A density functional investigation of the extradiol cleavage mechanism in non-heme iron catechol dioxygenases. *J. Biol. Inorg. Chem.* 2003; 8:409–418. [PubMed: 12761662]
38. Girerd J-J, Banse F, Simaan AJ. Characterization and properties of non-heme iron peroxy complexes. *Struct. Bonding.* 2000; 97:145–177.
39. Roelfes G, Vrajmasu V, Chen K, Ho R,YN, Rohde J-U, Zondervan C, La Crois R,M, Schudde E,P, Lutz M, Spek A,L, Hage R, Feringa B,L, Münck E, Que L Jr. End-on and side-on peroxy derivatives of non-heme iron complexes with pentadentate ligands: models for putative intermediates in biological iron/dioxygen chemistry. *Inorg. Chem.* 2003; 42:2639–2653. [PubMed: 12691572]
40. Karlsson A, Parales JV, Parales RE, Gibson DT, Eklund H, Ramaswamy S. Crystal structure of naphthalene dioxygenase: Side-on binding of dioxygen to iron. *Science.* 2003; 299:1039–1042. [PubMed: 12586937]
41. Neibergall MB, Stubna A, Mekmouche Y, Münck E, Lipscomb JD. Hydrogen peroxide dependent cis-dihydroxylation of benzoate by fully oxidized benzoate 1,2-dioxygenase. *Biochemistry.* 2007; 46:8004–8016. [PubMed: 17567152]

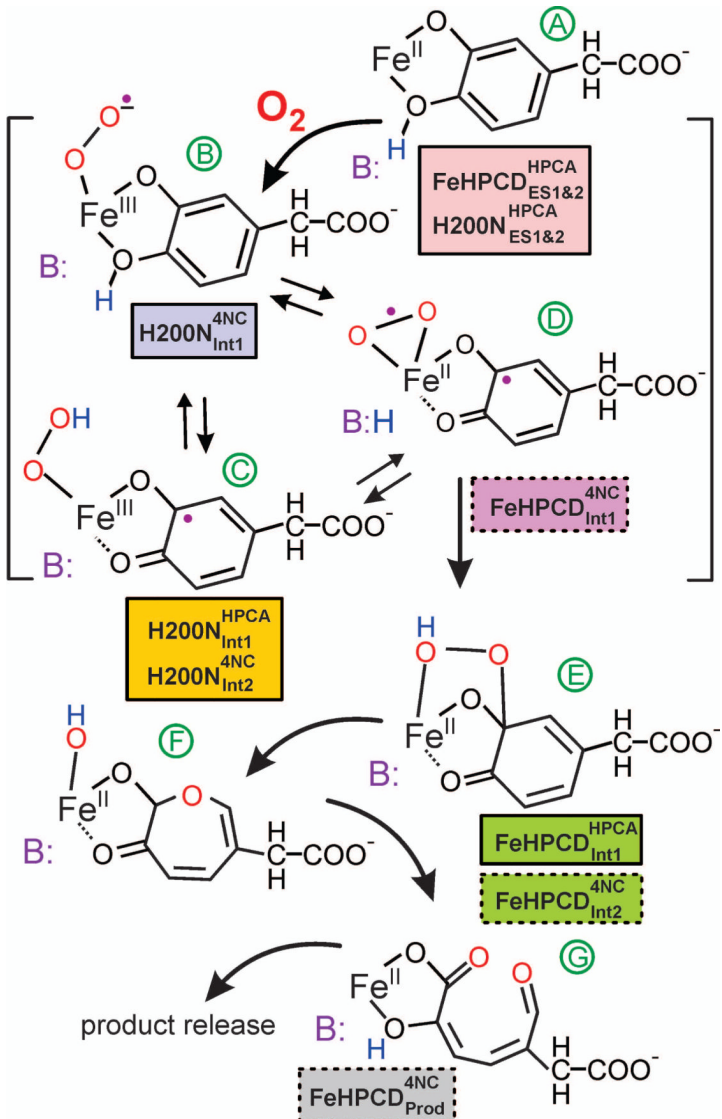


**Scheme 1. Proposed Reaction Mechanism for Extradiol Dioxygenases**

For the studies described here, R is either -CH<sub>2</sub>COO<sup>-</sup> (HPCA) or -NO<sub>2</sub> (4NC). In the case of 4NC, the substrate is fully deprotonated, so the proton required for catalysis must derive from solvent.

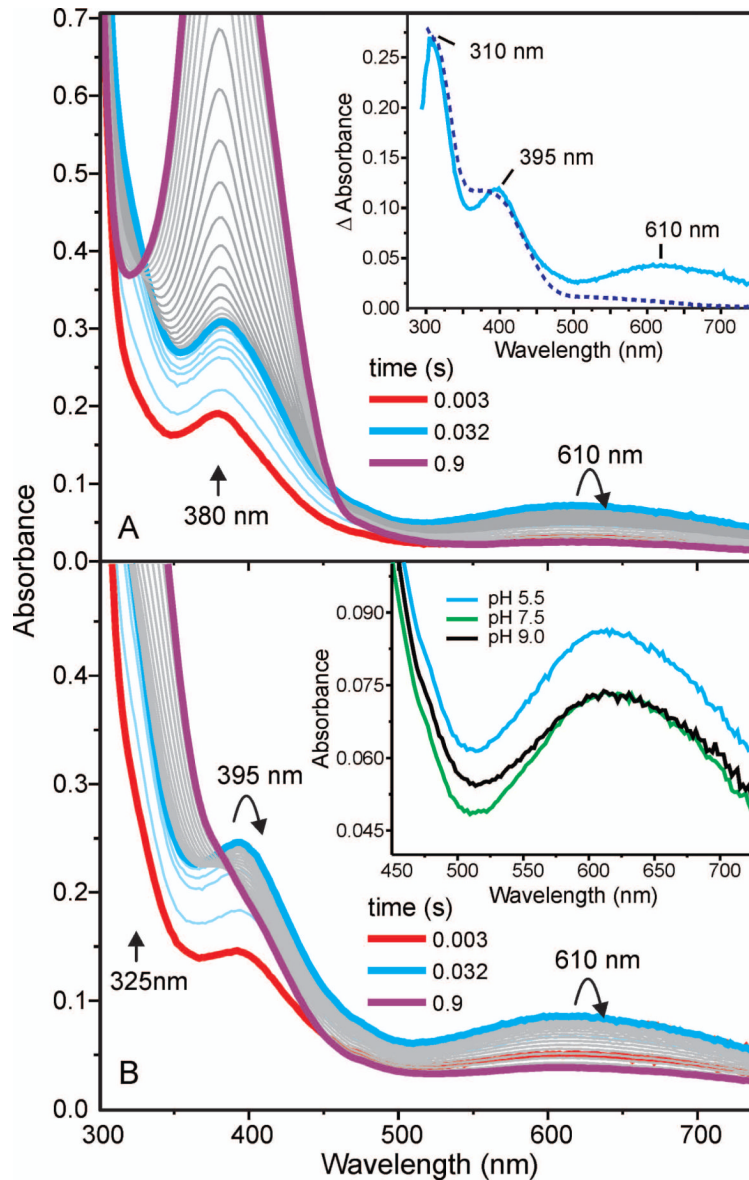
**Scheme 2.**

Kinetic Model from Stopped-flow Studies of the H200N-HPCA + O<sub>2</sub> Reaction.

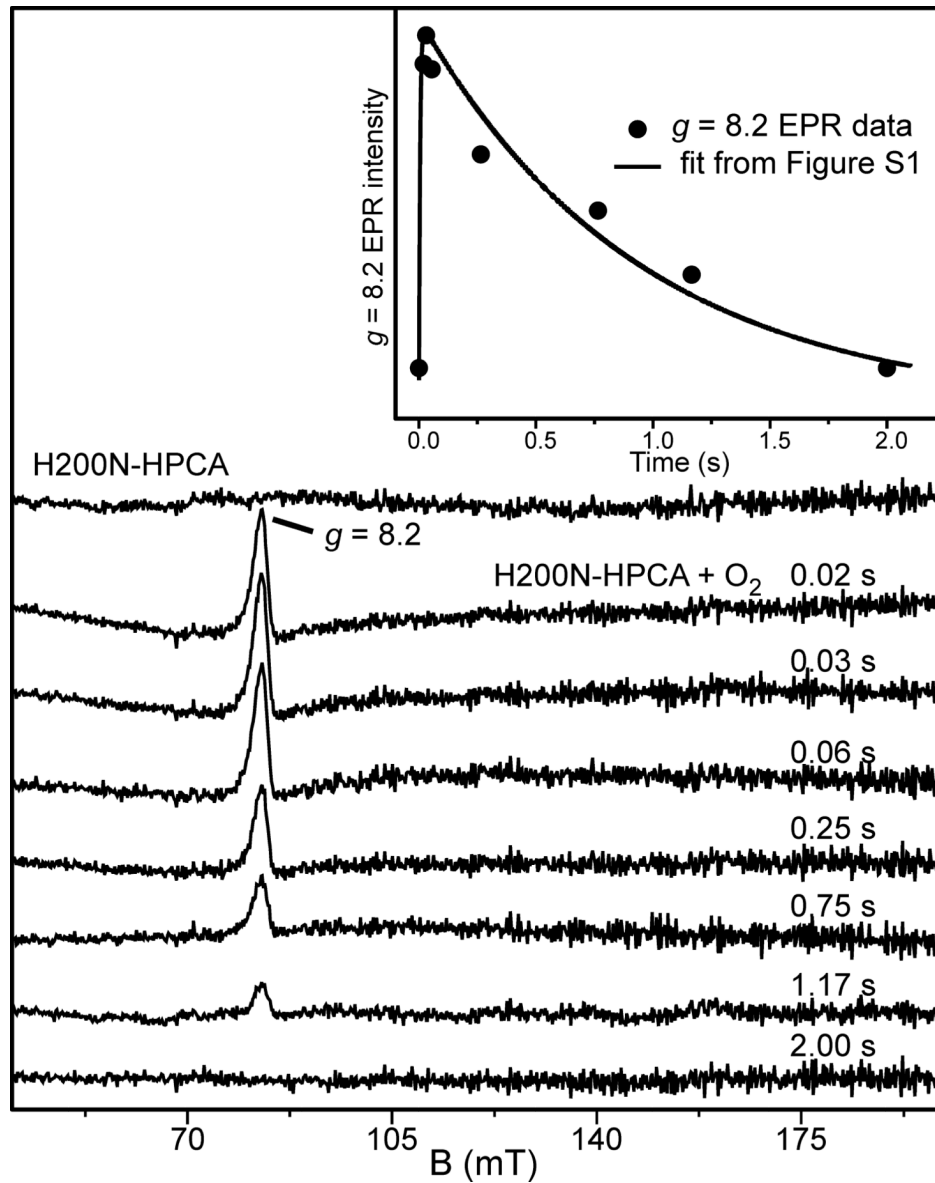


### Scheme 3. Intermediates from the FeHPCD and H200N Turnover Cycles

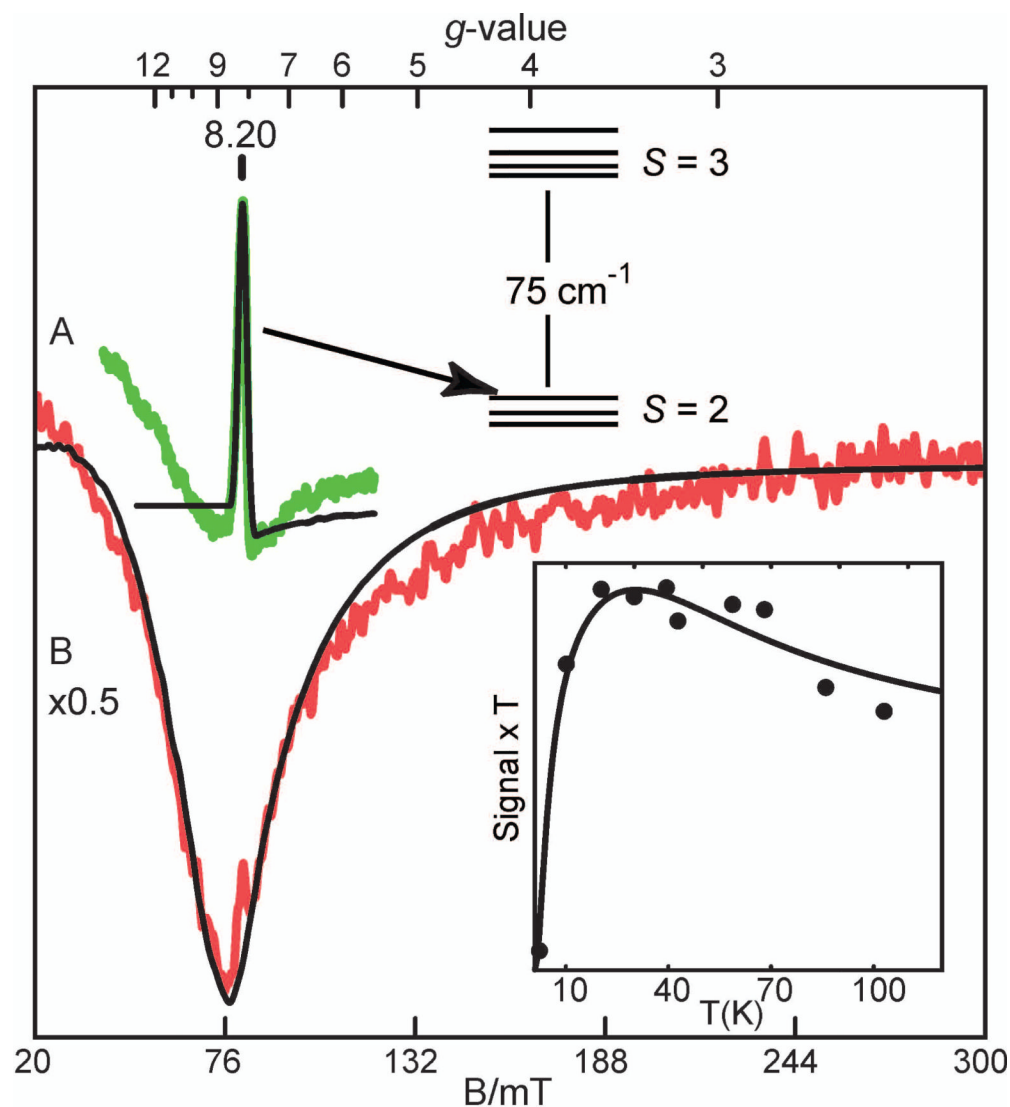
The intermediates shown are those proposed for the FeHPCD reaction with HPCA as the substrate. The colored boxes identify trapped intermediates that either correlate exactly with or are similar to these intermediates. The boxes with solid borders identify intermediates from solution RFQ studies reported here and in a previous study,<sup>19</sup> while those with dashed borders are from crystal structures reported previously.<sup>12</sup>



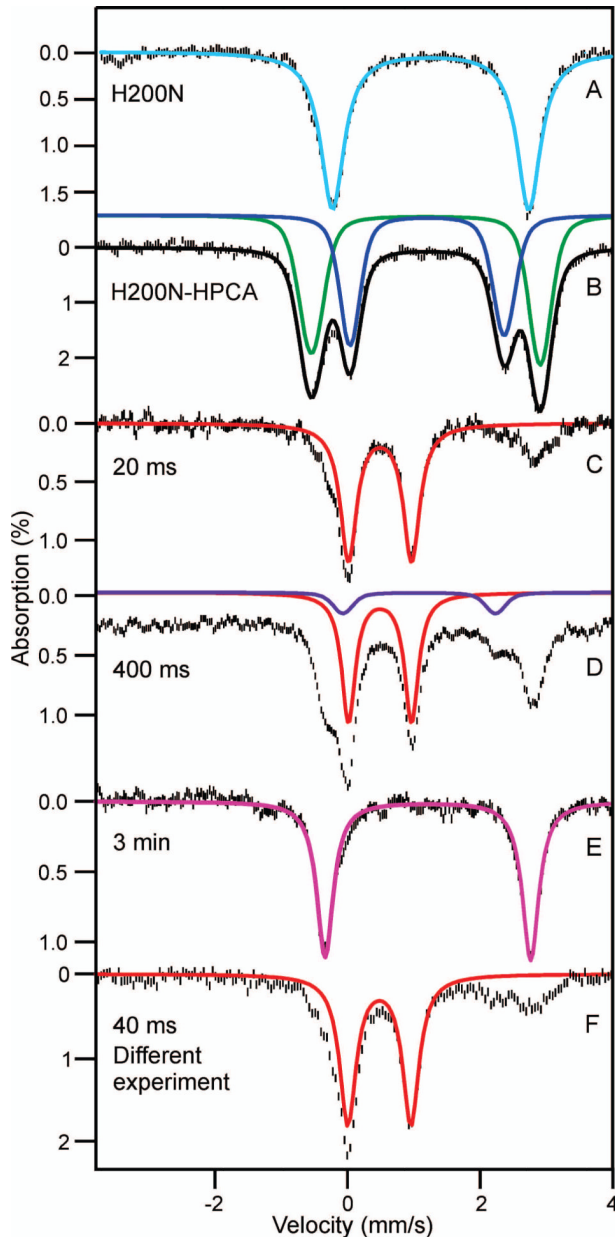
**Figure 1.** H<sub>2</sub>O<sub>2</sub>-HPCA + O<sub>2</sub> reaction monitored by stopped-flow. Panel A shows diode array spectra recorded between 3 ms and 2 s after mixing stoichiometric 640  $\mu$ M (sites) H<sub>2</sub>O<sub>2</sub>-HPCA anaerobic complex with O<sub>2</sub>-saturated buffer (~ 1.8 mM) (1:1) at 4 °C in 200 mM MOPS pH 7.5 (2 mm pathlength). The thick line spectra are for the specific times shown. Thin line cyan, 3 – 32 ms; gray, 32 ms – 2 s. The *inset* shows spectrum that results from subtracting the spectrum at 3 ms from that at 32 ms (cyan) and the spectrum of HPCA quinone produced by treatment of HPCA with mushroom tyrosinase (blue, dashed). Panel B shows the time course of the same reaction as in Panel A, but in 200 mM MES buffer pH 5.5. *Inset:* Comparison of the spectra of the 610 nm feature formed at pH 5.5, 7.5, and 9.0.

**Figure 2.**

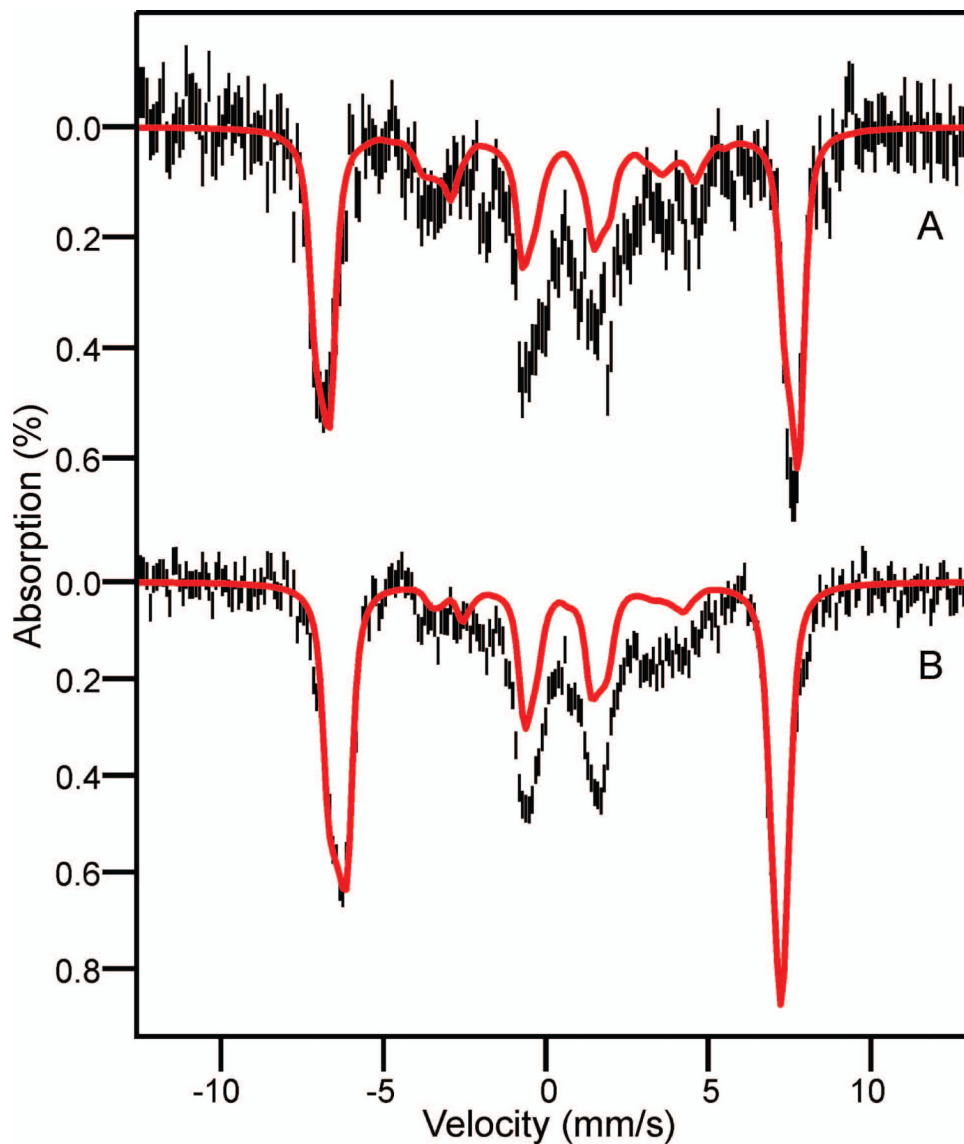
Time dependent parallel mode EPR spectra from the H200N-HPCA + O<sub>2</sub> reaction. Parallel mode EPR spectra in the  $g = 8$  region of RFQ samples frozen between 0 (top, unreacted) and 2 s after mixing 1.65 mM anaerobic H200N-HPCA complex with O<sub>2</sub>-saturated buffer (1:1) at 4 °C in 200 mM MOPS buffer, pH 7.5 are shown. EPR conditions: Frequency 9.35 GHz; microwave power, 50.4 mW; modulation amplitude, 1 mT, and temperature 50 K. *Inset:* Time course of the  $g = 8.2$  signal intensity (●). The solid line is the fit to the *optically* monitored time course at 610 nm from Figure S1.



**Figure 3.**  
Parallel-mode EPR spectra (colored) and simulations (black) for H200N-HPCA frozen 40 ms after reaction with O<sub>2</sub> at temperatures of (A) 10 K and (B) 2 K. Prior to mixing with O<sub>2</sub>-saturated buffer: 1.5 mM H200N-HPCA, 200 mM MOPS buffer pH 7.5. Simulation parameters: A:  $S_1 = 5/2$ ,  $S_R = 1/2$ ,  $J = +25 \text{ cm}^{-1}$ ,  $D_1 = 1 \text{ cm}^{-1}$ ,  $E/D_1 = 0.12$ ,  $g_{1z} = 2.015$ ,  $g_{Rz} = 2.00$ . B:  $S = 2$ ,  $D = -4 \text{ cm}^{-1}$ ,  $E/D = 0.15$ ,  $g_z = 2.00$ . EPR conditions: microwaves, 20 mW (A), 0.2 mW (B) at 9.29 GHz; modulation, 1.0 mT. The intensity of B has been reduced by a factor of 2. The *inset* shows a plot of signal times temperature for the  $g = 8.2$  feature and a theoretical fit to this intensity.

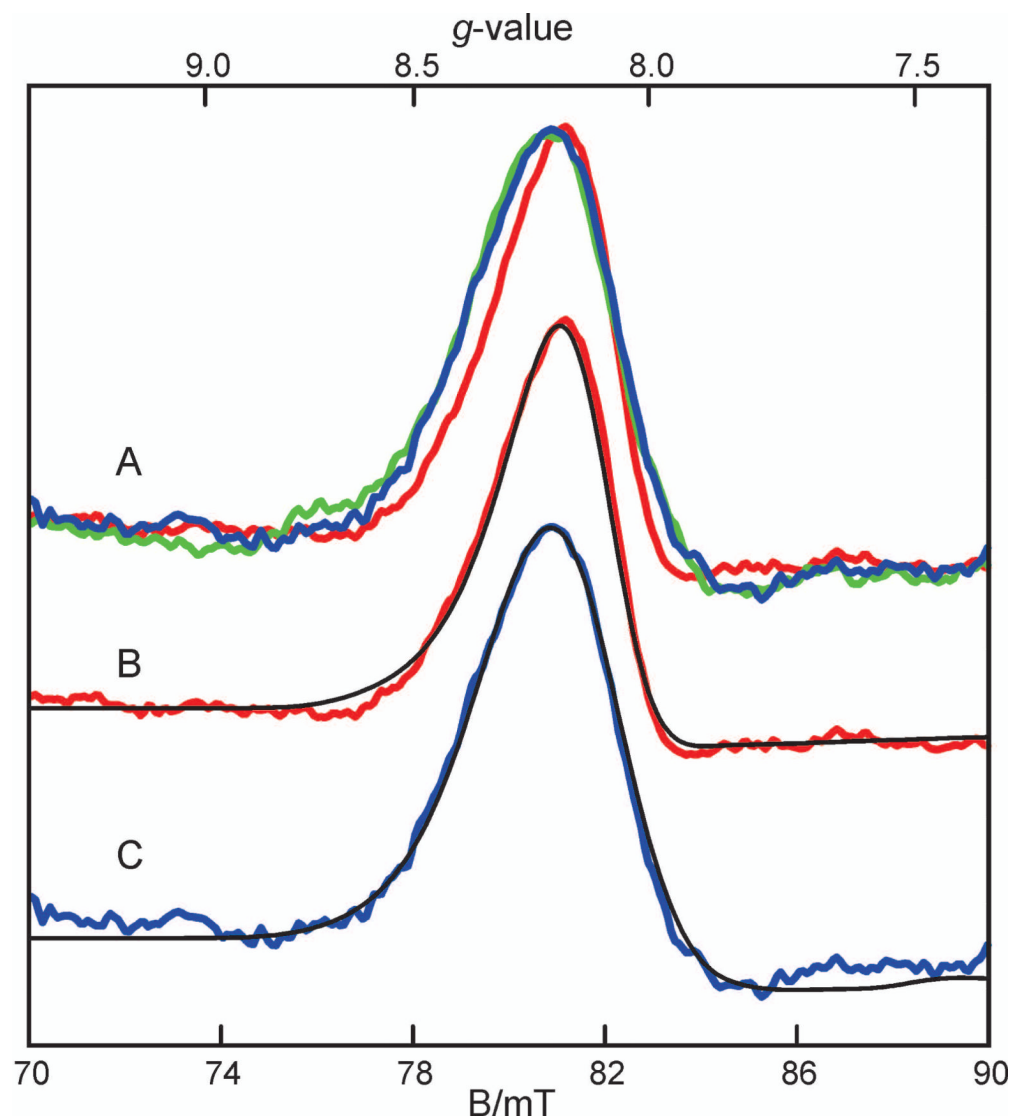
**Figure 4.**

4.2 K zero field Mössbauer spectra of H200N-HPCA complexes. (A) H200N, 0.9 mM at pH 7.5 in 200 mM MOPS buffer. The colored line is a simulation. (B) Stoichiometric (sites) H200N-HPCA complex, 1.54 mM, at pH 7.5 in 200 mM MOPS buffer. Simulations of the doublets of the two enzyme-substrate complexes,  $H200N_{ES1}^{HPCA}$  (green) and  $H200N_{ES2}^{HPCA}$  (blue), are depicted by the colored lines. The black line represents the sum of the two species. (C-E) Reaction of 1.48 mM H200N-HPCA with O<sub>2</sub>-saturated buffer (1:1). For the RFQ samples quenched at (C) 20 ms and (D) 400 ms, we have outlined in red the spectrum of the intermediate,  $H200N_{Int1}^{HPCA}$ . (E) Sample frozen (not by RFQ) at 3 min representing the end of the reaction. The colored line is a simulation of the spectrum. (F) B = 0 spectrum of the RFQ sample of Figure 5 prepared in a different experiment under the same conditions.

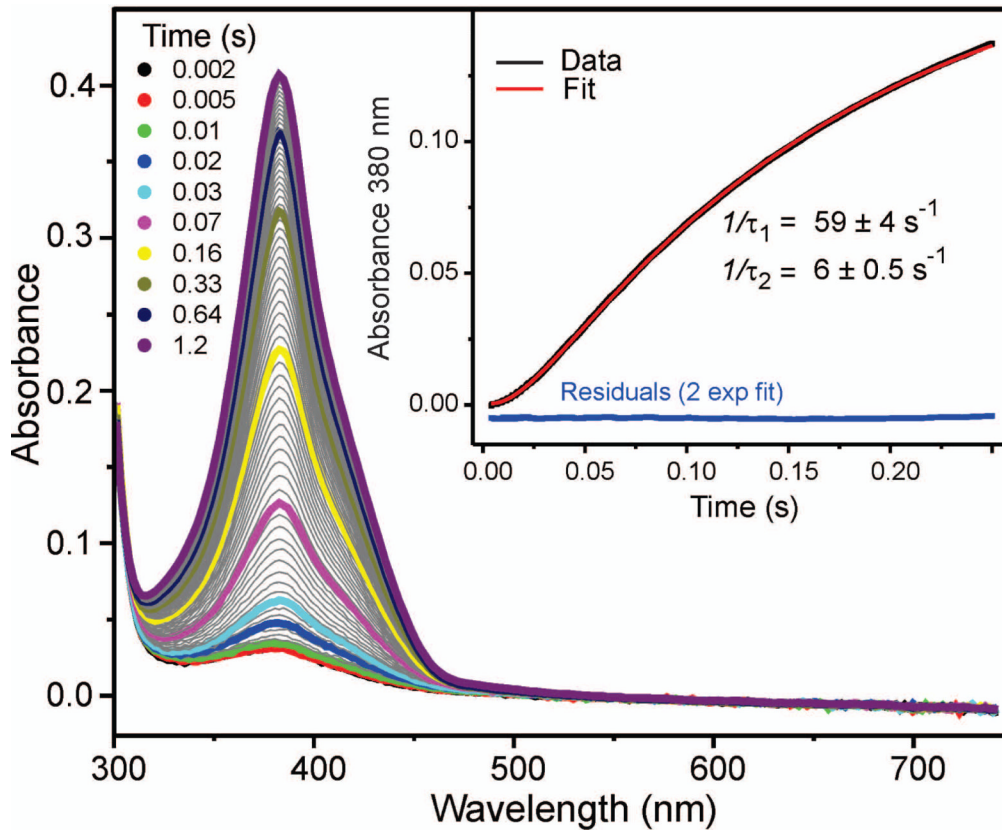


**Figure 5.**

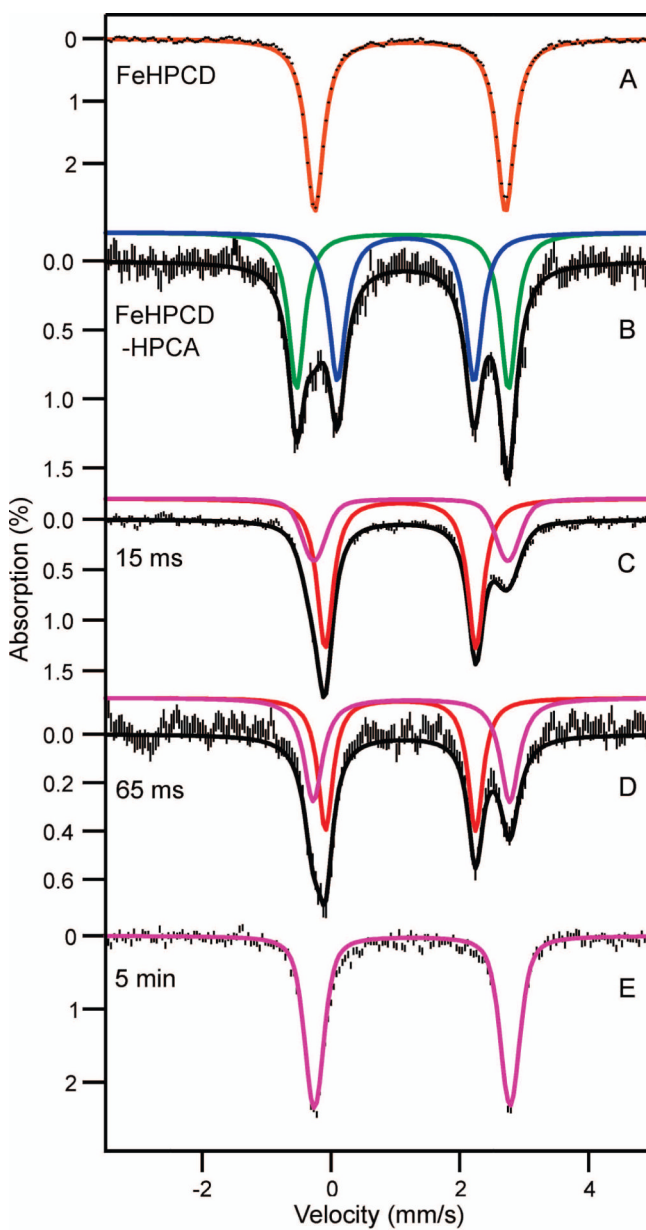
4.2 K Mössbauer spectra of  $\text{H}_2\text{O}_2\text{N}_{\text{Int}1}^{\text{HPCA}}$  recorded in parallel applied magnetic fields of (A) 4.0 T, and (B) 8.0 T. The central features of the spectra have unresolved contributions from the “splashed” ferrous contaminant. The red lines, drawn to represent 70 % of total Fe, are WMOSS spectral simulations based on eq 1 using the parameters listed in Table 1. This is the sample from Figure 4F.

**Figure 6.**

(A) EPR spectra of isotopically enriched H<sub>2</sub>O<sub>2</sub>N-Int<sup>1</sup>HPCA prepared with (red) natural abundance isotopes, (blue) 70% enriched <sup>17</sup>O<sub>2</sub>, (green) HPCA enriched to 68% with <sup>17</sup>O at the C3 OH functional group. Samples were prepared as described in Figure 2. Conditions before mixing: 1.65 mM H<sub>2</sub>O<sub>2</sub>N-HPCA complex, saturated O<sub>2</sub>-containing buffer, 200 mM MOPS pH 7.5 and 4 °C. EPR conditions: Frequency 9.29 GHz; microwave power, 20 mW; modulation, 1.0 mT, temperature, 10 K. The simulations of natural abundance (B) and 70% enriched <sup>17</sup>O<sub>2</sub> (C) samples are for S = 2, D = 1.3 cm<sup>-1</sup>, E/D = 0.12, with A<sub>z</sub><sup>O,c</sup> of 0 (B) or 17 MHz (C).



**Figure 7.** FeHPCD-HPCA + O<sub>2</sub> reaction monitored by stopped-flow. Diode array spectra recorded between 4 ms and 2 s after mixing 100 μM (based on active sites) stoichiometric, anaerobic FeHPCD-HPCA complex with O<sub>2</sub> saturated buffer (~1.8 mM) at 4 °C in 200 mM MOPS pH 7.5 (2 mm pathlength). Inset: Reaction monitored by single wave stopped-flow spectroscopy at 380 nm. In the time range shown, the data (black line) can be fit to a sum of two exponential terms (red line) with the reciprocal relaxation times shown.

**Figure 8.**

Mössbauer spectra from the FeHPCD-HPCA + O<sub>2</sub> reaction recorded at 4.2K for B = 0. (A): FeHPCD, (B): The anaerobic FeHPCD-HPCA complex, (C): FeHPCD-HPCA + O<sub>2</sub> at 15 ms after mixing with O<sub>2</sub>, (D): FeHPCD-HPCA + O<sub>2</sub> at 65 ms after mixing with O<sub>2</sub>, (E): 5 min after mixing. Conditions before mixing: ~ 1.8 mM enzyme-substrate complex, 200 mM MOPS, pH 7.5, and 4 °C all reactions. For (A) the sample concentration was ~ 0.9 mM.

**Table 1**  
Spin-Hamiltonian parameters for exchange coupled intermediates from EPR (italics) and Mössbauer spectroscopy.

Species	$\delta$ (mm/s)	$\Delta E_Q$ (mm/s)	$J$ (cm $^{-1}$ )	$D_1$ (cm $^{-1}$ )	$(E/D)_1$	$A_0/g_{\text{eff}}n$ (T)	$A^O$ (MHz)	$^{17}\text{O}_2$	$^{17}\text{O}$ -HPCA	Ref
$\text{H}_2\text{OON}_{\text{Int}1}^{4\text{NC}}$	0.5	-0.33 <sup>a</sup>	-3 <sup>a</sup>	+6(2) <sup>a</sup>	-0.59 -0.48	0.20 0.20	-21.4(2)	180	N/A	<sup>19</sup>
$\text{H}_2\text{OON}_{\text{Int}2}^{4\text{NC}}$	0.49	0.87	-7.2	+40(10)	+0.67 +0.50 0.13	0.11 0.13	-21.5(2)	<5	N/A	<sup>19</sup>
$\text{H}_2\text{OON}_{\text{Int}1} \text{ HPCA}$	0.48(l)	0.95(2)	+3 <sup>a</sup>	+25(5)	+1.1 <sup>b</sup> +1.1	0.12 0.12	-21.5(2)			This work
$\text{H}_2\text{OON}_{\text{Int}1} \text{ HPCA, } S = 2 \text{ Hamiltonian}$	0.48	0.95	+3		1.5	0.12	-25.1	17	17	This work

<sup>a</sup>  $\eta = +3$  and  $\eta = -3$  imply that the EFG is axial around the x and y axis, respectively.

<sup>b</sup> The last row lists the parameters as evaluated for  $S = 2$  multiplet of the coupled system. The full Hamiltonian is given in eq 2. This representation must be used for analysis of the  $^{17}\text{O}$  data (an explanation is given in the text). If the radical were on the O<sub>2</sub> moiety, the coupling in the uncoupled representation would be  $6 \times 7 = 102$  MHz which can be compared with the 180 MHz reported for  $\text{H}_2\text{OON}_{\text{Int}1}^{4\text{NC}}$ .

**Table 2**

Comparison of quadrupole splitting and isomer shift parameters for the Mössbauer spectra of FeHPCD and its variants and complexes.

Species	$\Delta E_Q$ (mm/s)	$\delta$ (mm/s)	% present in sample at maximum
FeHPCD	2.97(3)	1.23(2)	>90
H200N	3.01(3)	1.24(2)	>90
H200N-4NC <sup>a</sup>	3.57	1.12	>90
FeHPCD <sub>ES1</sub> <sup>HPCA</sup> FeHPCD <sub>ES2</sub> <sup>HPCA</sup>	3.29(3) 2.18(3)	1.14(2) 1.18(2)	55 45
H200N <sub>ES1</sub> <sup>HPCA</sup> H200N <sub>ES2</sub> <sup>HPCA</sup>	3.45(3) 2.32(3)	1.16(2) 1.20(2)	60 40
FeHPCD <sub>Int1</sub> <sup>HPCA</sup>	2.33(3)	1.08(2)	~ 95 <sup>b</sup>
H200N <sub>Int1</sub> <sup>HPCA</sup>	0.95(2)	0.48(1)	~ 95 <sup>b</sup>
H200N <sub>Int2</sub> <sup>HPCA</sup>	~2.30	~1.10	~ 10

<sup>a</sup>From Ref.<sup>19</sup>

<sup>b</sup>After correction for material splashed from the rapid freezing surface at high ram velocities